

Rockslide tsunamis in complex fjords: From an unstable rock slope at Åkerneset to tsunami risk in western Norway



C.B. Harbitz^{a,b,c,*}, S. Glimsdal^{a,b,c}, F. Løvholt^{a,b,c}, V. Kveldsvik^b, G.K. Pedersen^{a,c}, A. Jensen^a

^a Department of Mathematics, University of Oslo, PO Box 1053 Blindern, 0316 Oslo, Norway

^b Norwegian Geotechnical Institute (NGI), PO Box 3930 Ullevaal Stadion, N-0806 OSLO, Norway

^c International Centre for Geohazards (ICG), c/o NGI, PO Box 3930 Ullevaal Stadion, N-0806 OSLO, Norway

ARTICLE INFO

Article history:

Received 17 December 2012

Received in revised form 2 February 2014

Accepted 5 February 2014

Available online xxxx

Keywords:

Rockslide
Tsunami
Risk
Åknes
Åkerneset
Hegguraksla

ABSTRACT

An unstable rock volume of more than 50 million m³ has been detected in the Åkerneset rock slope in the narrow fjord, Storfjorden, Møre & Romsdal County, Western Norway. If large portions of the volume are released as a whole, the rockslide will generate a tsunami that may be devastating to several settlements and numerous visiting tourists along the fjord. The threat is analysed by a multidisciplinary approach spanning from rock-slope stability via rockslide and wave mechanics to hazard zoning and risk assessment.

The rockslide tsunami hazard and the tsunami early-warning system related to the two unstable rock slopes at Åkerneset and Hegguraksla in the complex fjord system are managed by Åknes/Tafjord Beredskap IKS (previously the Åknes/Tafjord project). The present paper focuses on the tsunami analyses performed for this company to better understand the effects of rockslide-generated tsunamis from Åkerneset and Hegguraksla. Two- and three-dimensional site-specific laboratory experiments are conducted to study the generation, propagation, and run-up of the wave for several potential rockslide scenarios from Åkerneset. Furthermore, the two models GloBouss and DpWaves are applied for numerical simulations of the generation/propagation phase and a third model MOST is applied for numerical simulations of the near-shore propagation and inundation of the wave in selected locations. Strong emphasis is put on verification, validation, and sensitivity of the numerical models. The best match between the numerical simulations and the laboratory experiments is found for the larger scenarios with the linear dispersive solution for the propagation phase; the corresponding calculated run-up values are remarkably similar to the ones observed during the laboratory experiments.

During the risk assessment it was found that the rockslide tsunami hazard (probability of impact) is higher than accepted by the Norwegian Planning and Building Act. This should at that time prevent any further development in all the exposed areas of the entire fjord system. The Act is today altered to open for specified further development in the various hazard zones. The results of the tsunami analyses are applied in risk management in terms of hazard map production and land-use planning. Two failure scenarios for each of the two unstable rock slopes are designed for the hazard zoning. The larger and less probable scenarios (1 in 5000 years) are applied for evacuation zones and routes, while the smaller and more probable scenarios (larger than 1 in 1000 years) are applied for location and design of less critical facilities accepted in the inundation zone.

© 2014 Elsevier B.V. All rights reserved.

1. Introduction

1.1. Background

Rockslides plunging into fjords, lakes, or artificial reservoirs can generate huge, destructive waves. Tsunamis may cause large oscillations in basins or fjords, causing a series of incident waves. The first wave is not necessarily the largest. Wave activity may last for hours. Examples of well-documented rockslides in fjords include the 1934 Tafjord event

in Norway (Braathen et al., 2004; Furseth, 1985, 2009; Harbitz et al., 1993; Jørstad, 1968) and the 1958 Lituya Bay event in Alaska (Fritz et al., 2009; Miller, 1960) that caused maximum run-up heights of more than 60 m and 500 m, respectively. A well-known example of a rockslide into a reservoir is the disastrous 1963 Vaiont Dam event in Italy, where a 240 Mm³ rockslide caused a wave that reached a height of more than 250 m around the dam and killed about 2000 people living in the downstream villages (Ghirotti, 2012; Kiersch, 1964; Müller, 1964, 1968).

Norway experienced three major tsunami disasters due to subaerial rockslides plunging into water in the twentieth century, Loen (in 1905 and 1936) and Tafjord (in 1934; Figs. 1–2). The three events caused in total 174 casualties. The maximum run-up heights (water level above equilibrium along the line of maximum inundation distance) ranged

* Corresponding author at: Norwegian Geotechnical Institute (NGI), PO Box 3930 Ullevaal Stadion, N-0806 OSLO, Norway. Tel.: +47 22 02 30 00.

E-mail address: carl.bonnie.harbitz@ngi.no (C.B. Harbitz).



Fig. 1. The fjord Tafjorden with the village Tafjord (lower left foreground) and the 1934 rockslide scar (right middle ground). Photo: Fjellanger Widerøe A.s. © Normanns Kunstforlag A/S.

from 40.5 to 74.2 m. Historical records (from the last 400 years, say) indicate that Norway has experienced about two to three catastrophic events every century, causing in total about 250 tsunami fatalities. In addition, several smaller events with severe damage, but none or very few tsunami fatalities, have occurred. At least twelve large rockslides have occurred in the inner Storfjorden area, Møre & Romsdal County, Western Norway, in the same period, causing in total 68 tsunami fatalities (Blikra et al., 2006). It is expected that a future event will be much more disastrous than the historic ones owing to strongly increased coastal population, development, tourism, and other activity along the shoreline. Development in the Storfjorden area that is exposed to possible rockslide tsunamis has increased further since the inner part Geirangerfjorden was inscribed on the UNESCO World Heritage List in 2005. The Geirangerfjord is visited by 150–200 cruise ships and more than 700 000 tourists each year (www.visitnorway.com). Additional information on the hazard related to rockslides and tsunamis in the Norwegian fjords is presented by Blikra et al. (2005, 2006).

The present paper starts with a discussion of the tsunami hazard in the NE Atlantic including the Norwegian fjords (Section 1.2). Then follows a presentation of the Åknes/Tafjord project managing the rockslide tsunami hazard formed by the two unstable rock slopes at Åkerneset and Hegguraksla in the narrow fjord system, Storfjorden, Møre & Romsdal County, Western Norway (Section 1.3). In this context, an overview of other projects worldwide with relevance for rockslide tsunami risk assessment and management is also presented (Section 1.4). The stability analyses and the monitoring of the Åkerneset and Hegguraksla rock slopes that constitute the basis for the design of the rockslide scenarios and the tsunami early-warning system are discussed in Section 2. The focus of the paper is the site-specific physical and numerical modelling performed for the Åknes/Tafjord project to better understand the effects of rockslide-generated tsunamis from Åkerneset and Hegguraksla (Sections 3 and 4). The main results of the numerical modelling applied for the hazard zoning are presented in Section 5. The applications in terms of risk analysis and assessment are briefly



Fig. 2. Left: Remnants of the village Tafjord after the 1934 rockslide tsunami catastrophe (from Furseth, 1985). The stone Haugsteinen on which six persons saved their lives is located on the little hill in the left part of the picture (indicated by the arrow). Right: Close-up of Haugsteinen; the memorial to the 1934 Tafjord catastrophe to the right.

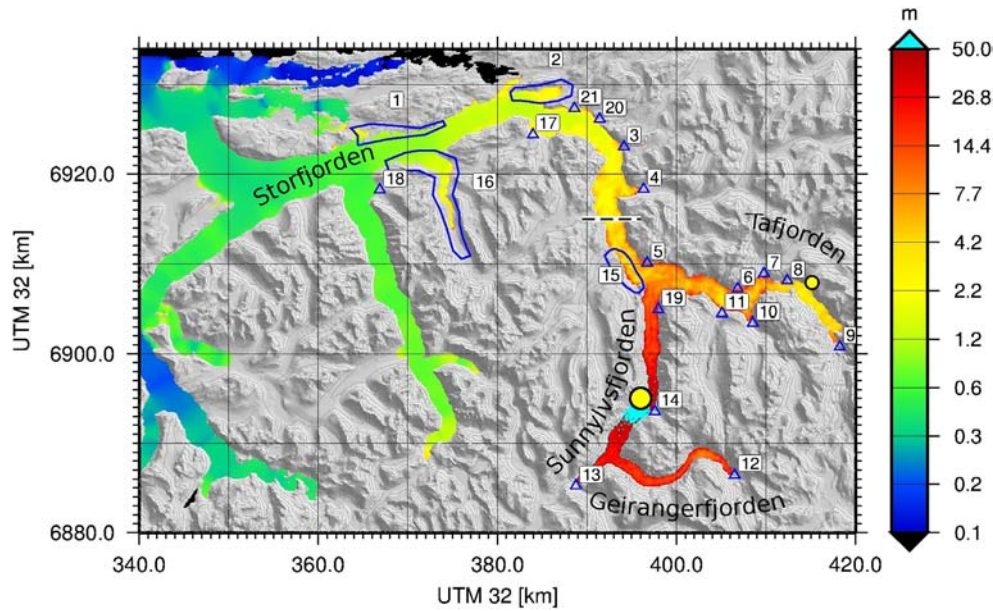


Fig. 3. Overview of all locations for hazard zoning with enumeration (marked by triangles for smaller and polygons for larger areas). Names and maximum calculated run-up heights for all these locations are listed in Table 1. Names of the various branches of the inner fjord system are shown. The colours represent maximum calculated surface elevation in metres for scenario 1C from Åkerneset (nominal probability between 1 in 1000 and 1 in 5000 years). The location of the Åkerneset and the Hegguraksla rock slopes is indicated by bigger and smaller yellow bullets, respectively. The dotted line defines inner and outer parts of Storfjorden with regard to applied bathymetries (see Section 4.1).

described in Section 6 to put the whole thing into perspective and to emphasize the need for and the usefulness of the modelling. Finally, the prospects for ongoing further studies are included in the concluding remarks (Section 7).

1.2. Tsunami hazard in the Northeast Atlantic

Within the framework of the EU project TRANSFER (Tsunami Risk And Strategies for the European Region, www.transferproject.eu), the potential tsunamigenic sources in the NE Atlantic were assessed for a first screening of regional tsunami hazard. Both near-field and far-field sources were considered. Based on modelling and evaluation of the corresponding tsunami scenarios, potential rockslides located in the fjords of Western Norway were considered the only high risk tsunamigenic sources in the NE Atlantic (the fjords in Greenland were not investigated). Submarine landslides off the Norwegian continental margin, rockslides in Northern Norway, as well as earthquakes off the Portuguese coastline were identified as sources constituting moderate tsunami hazard (Harbitz et al., 2009). Tsunamigenic earthquakes in the North Sea, the Norwegian Continental Margin, and the Norwegian–Greenland Sea were considered non-critical (Bungum and Lindholm, 2007). The Jan Mayen and Iceland volcanic sources, the landslide sources north of Svalbard (Vanneste et al., 2010) as well as the Grand Banks, Canary Islands (Løvholt et al., 2008), Cape Verde, and Caribbean far-field (Harbitz et al., 2012) sources were considered non-critical with regard to tsunami hazard in the NE Atlantic. It should be noted that important segments of the continental margins surrounding the northern North Atlantic and Arctic Ocean are not mapped in sufficient detail.

In the inner part of the fjord Storfjorden, 108 rockslide deposits have been mapped on the fjord bottom. Twenty-five events occurred during the deglaciation (12 500–10 000 ^{14}C years or 14 500–11 500 calendar years BP). Twenty-one rockslides are equal to or larger than the 1934 Tafjord rockslide, but only six out of these occurred during the Holocene (after 10 000 ^{14}C years or 11 500 calendar years BP). The rockslide activity was especially high shortly after the final deglaciation, ca. 10 000–9000 ^{14}C years or 11 500–10 200 calendar years BP (Blikra et al., 2006; NGU, 2009a), likely as a result of stronger isostatic landlift, more earthquakes, steeper reliefs, and permafrost melting (Vorren et al.,

2008). Subsequently, the distribution of events has been relatively constant, with five to eight events per 1000 years for the entire fjord system. The highest activity is found in Geirangerfjorden (Fig. 3), with one rockslide every 350 years. However, the average volume of the rockslides is here smaller than in other fjords. In the fjord Tafjorden, the frequency is one rockslide every 650 years, in Sunnlyvsfjorden one rockslide every 1300 years, and in Storfjorden from Stordal to the mouth of Sunnlyvsfjorden one rockslide every 3000 years. The largest rockslide deposit (180 Mm³) is found in Sunnlyvsfjorden slightly north of Åkerneset (NGU, 2009a). The numbers clearly demonstrate the need for further investigations of rock-slope stability and tsunamis in the fjords. Moreover, possible future climate changes implying higher temperatures combined with more frequent and extreme situations of intense precipitation (Alfnes and Førland, 2006; Benestad, 2013; Dyrørdal et al., 2011, 2012; Engen-Skaugen and Førland, 2011; Hanssen-Bauer et al., 2009; Hov et al., 2013; NGI, 2013a) may increase the rockslide frequency in Norway. Classification of hazard and risk related to unstable rock slopes and potential tsunamis in Norwegian fjords are further discussed by Hermanns et al. (2013a).

1.3. The Åknes/Tafjord project

Owing to the need for risk assessment and management in Storfjorden, the Åknes/Tafjord project (presently the Åknes/Tafjord Beredskap IKS¹; www.aknes.no) was established in 2004 as a research, monitoring, and early-warning project related to large unstable rock slopes and their consequences in terms of tsunamis. The uniquely multidisciplinary assessment of rockslide tsunami hazard and risk in a complex fjord system comprises five main aspects: 1) geological and geotechnical fieldwork as well as numerical analyses to assess the stability of the rock slopes; 2) statistical analysis for probability of release and for run-out distance of the rockslides; 3) numerical simulations and laboratory experiments of rockslide dynamics, and of tsunami generation, propagation, and inundation; 4) hazard and risk analyses; and finally 5) risk assessment and management including the establishment

¹ IKS is the Norwegian acronym for 'interkommunalt selskap' (inter-municipal company).



Fig. 4. The Åkerneset rock slope seen from the fjord Sunnlyvsfjorden. Scenario 1C (54 Mm³, nominal probability between 1 in 1000 and 1 in 5000 years) comprises approximately the whole shaded area. Scenario 2B (18 Mm³, nominal probability larger than 1 in 1000 years) comprises the part of the shaded area above the black line. Background photo by courtesy of Åknes/Tafjord Beredskap IKS.

of a preparedness centre for rock-slope monitoring, early-warning systems, public awareness, evacuation plans, and land-use planning. Beyond the obvious objective of providing input to the county/municipality preparedness programme in terms of rock-slope stability analysis, criteria for alert levels and distribution of warning, tsunami hazard zoning, etc., objectives have also been to establish methodologies and recommended practice for future applications in other places (Section 1.4).

Table 1

Calculated rockslide-generated tsunami run-up heights in metres above current mean sea level (MSL) for the four modelled rockslide scenarios. Location numbers refer to Fig. 3. The heights include the effect of a sea level rise of 0.7 m.

Location		Scenarios			
		Åkerneset		Hegguraksla	
Name	number	1C	2B	H2	H3
Dyrkorn	3	3	2	–	–
Eidsdal	11	8	4	–	–
Fjora	8	6	3	17	20
Geiranger	12	70	30	–	–
Gravaneset	5	7	3	–	–
Hellesylt	13	85	35	–	–
Hundeidvik	18	2	1	–	–
Linge	6	6	3	–	–
Magerholm	1	3	1	–	–
Norddal	10	14	7	–	–
Oaldsbygda	14	100	70	–	–
Ramstadvika	17	3	2	–	–
Raudbergvika	19	13	6	–	–
Skardbøen	21	4	2	–	–
Stordal	4	8	4	–	–
Stranda	15	7	4	–	–
Sykkylvsfjorden	16	4	2	–	–
Tafjord	9	14	7	9	13
Vaksvik	20	5	3	–	–
Vallidal	7	7	3	6	8
Vegsundet	1	4	3	–	–
Vika	8	9	4	11	15
Ørskog	2	6	3	–	–

The tsunami analyses presented below are all produced for the Åknes/Tafjord project. They are made for a large set of rockslide scenarios (with corresponding annual probabilities of release) from the two rock slopes at Åkerneset and Hegguraksla. Inundation modelling and hazard zoning are performed for more than twenty locations, Fig. 3. The tsunami modelling results gained in the Åknes/Tafjord project provide a fruitful and immediate application of academic studies in consulting (ÅTB, 2011; NGI, 2010a). The same results have also been applied further in local analysis for other clients doing land-use planning or optimizing location and design of harbours and sea farming structures along Storfjorden (NGI, 2008a, 2008b, 2008c, 2010b, 2011a, 2011b, 2012, 2013b). It should be noted that tsunamis caused by possible rockslides in Storfjorden have also been studied in earlier projects initiated by the Stranda Municipality (NGI, 1991) and the Norwegian Natural Disaster Fund (NGI, 1992, 2003a).

1.4. Other projects with relevance for rockslide tsunami risk assessment and management

The experience on rockslide tsunami risk assessment and management gained from the Åkerneset and Hegguraksla rock slopes is presently utilized also in other places in Norway. The most relevant example is the Nordnes rock slope along the fjord Lyngen, Troms County, Northern Norway (Braathen et al., 2004; Lauknes et al., 2010; NGI, 2008d, 2010c, 2013c; NGU, 2009b; Nordvik et al., 2010). The authors are aware of only a few other projects worldwide including rockslide tsunami risk assessment and management in mountainous areas with fjords, lakes, or reservoirs. A larger number of additional projects include elements of rockslide tsunami risk assessment limited to analysis of rock-slope stability or rockslide mechanics, pure rock-slope monitoring, analyses of past rockslide tsunami events, or likelihood and hazard assessment of possible future events. Notably, the assessments often conclude that monitoring and warning systems are needed. Examples of projects including rock-slope analyses and long term monitoring with regard to possible rockslide tsunamis are given below.

Table 2

Parameter values and probabilities for all the scenarios applied for the hazard zoning (from ÅTB, 2011; NGI, 2014).

Scenario		Dimensions			Impact velocity	Volume	Annual probability
Location	Number	Height [m]	Width [m]	Length [m]	[m/s]	[10 ⁶ m ³]	
Åkerneset	1C	120	450	1000	45	54	1/1000–1/5000
	2B	80	450	500	45	18	>1/1000
Hegguraksla	H2	40	200	250	60	2	>1/1000
	H3	46	250	300	60	3.5	1/1000–1/5000

First, prior to the 1963 Vaiont Dam event, Italy (above), there was a concern about the stability of the southern bank of the dam. At the same time, laboratory experiments indicated that a wave generated by a landslide into the reservoir could top the crest of the dam. However, experts were ignored when stating that the entire valley side was unstable and likely to collapse into the reservoir if the filling were completed (http://en.wikipedia.org/wiki/Vajont_Dam). Impromptu slope stability monitoring of the bank was undertaken and displacements were observed whilst the reservoir was filled. Nevertheless, it was considered possible to control the landslide creep-rates by altering the water level of the reservoir whilst controlling the joint water thrust within the rock mass by means of drainage tunnels. A by-pass tunnel was constructed on the opposite (northern) bank such that if the landslide should divide the reservoir into two sections, the level of the lake could still be controlled (<http://www.landslideblog.org/2008/12/vaiont-vajont-landslide-of-1963.html>). The final attempt to control the landslide into the reservoir caused a wave that overtopped the dam by about 250 m (ten times higher than predicted). There is no known record of any warning or evacuation order being issued to the populace. The dam itself was largely undamaged and is still standing today. The by-pass tunnel is used for generation of hydroelectric power (http://en.wikipedia.org/wiki/Vajont_Dam). The tragic event illustrates the consequence of not heeding insights offered by modelling and monitoring, and the need to implement risk mitigation measures. For further details, see Semenza (2005) and Ghirotti (2012).

The natural 600-m-high Usoy landslide dam in the Pamir Mountain Range, eastern Tajikistan, is the highest dam in the world. It was formed when the 1911 Sarez earthquake triggered the landslide that blocked the Murghab River forming Lake Sarez that currently holds a volume of 17 km³ (Schuster and Alford, 2004). It is clear now that the dam is stable and cannot spontaneously collapse, but there is still a certain danger due to the seismicity of the region, catastrophic overtopping waves induced by the unstable right-bank masses, dam surface erosion caused by natural overtopping by the rising lake, internal erosion (piping), etc. However, the danger is lower than previously suspected (Droz and Spasic-Gril, 2006; Schuster and Alford, 2004; <http://www.sarez.tj>). Possible disaster scenarios could cause an uncontrolled increase in lake outflow or a dam breach/failure. A system monitoring landslide movements, seismic activity, lake level, abnormal waves, dam body movements, outflow discharge, flooding, and meteorological parameters integrated into an early-warning system was installed in 2004 (Droz and Spasic-Gril, 2006). The system is supposed to be operational until 2020 when it is hoped that there will be funds available to eliminate the risk associated with the dam, the reservoir, and the unstable slope by lowering the lake level (E. Dibiagio, pers. comm. 2011).

In Switzerland, the guidelines for the safety of the hydropower dams discuss the treat from rockslides, debris flows, snow avalanches, and related tsunamis (BWG, 2002a, 2002b). Hydropower reservoir-slope stability is assessed every five years and potentially unstable slopes are monitored. The dam freeboards are normally designed to cope with

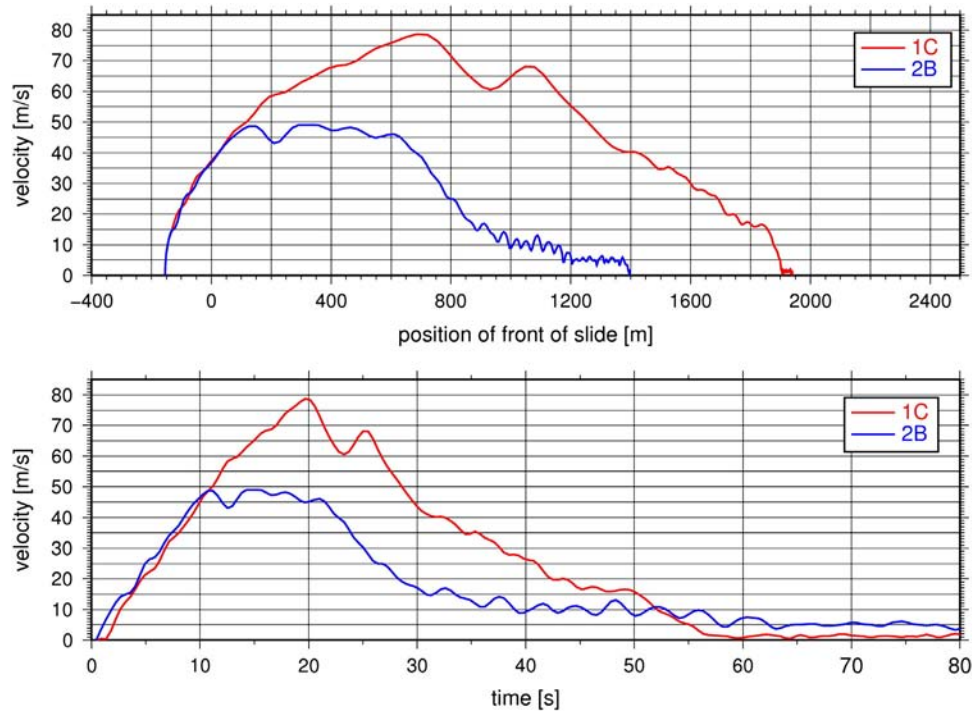


Fig. 5. Velocity progression as a function of front position of the rockslide (upper panel) and time (lower panel) for rockslide scenarios 1C (nominal probability between 1 in 1000 and 1 in 5000 years) and 2B (nominal probability larger than 1 in 1000 years) from Åkerneset, as measured in the laboratory experiments (transferred to full scale). Position = 0 in the upper panel corresponds to the shoreline.

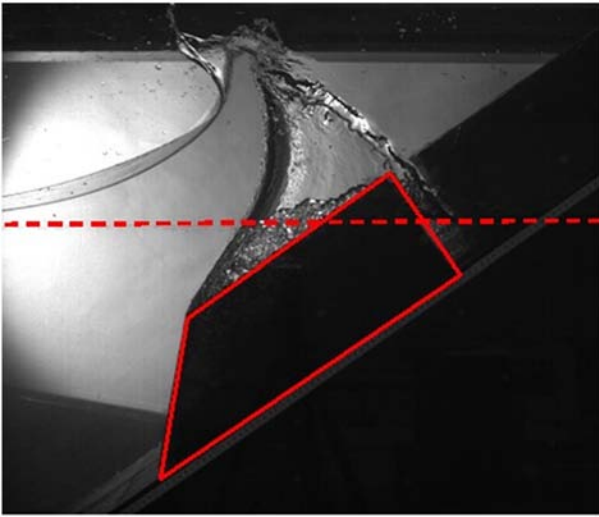


Fig. 6. Wave generation by a “rockslide box” (red trapezoid) at the Hydrodynamics Laboratory, University of Oslo. The box pushes the water up and forward, leaving a cavity above the box. The dashed line indicates equilibrium water level prior to impact. (For interpretation of the references to colour in this figure legend, the reader is referred to the web version of this article.)

rockslide tsunamis and the larger hydropower reservoirs (about 66) are equipped with alarms warning people downstream in case of uncontrolled water release (M. Wieland, pers. comm. 2011). In New Zealand, the movement rates of 17 landslides around Clyde dam reservoir have been monitored prior to, during, and since lake filling in 1992–93. The data provide a record longer than 20 years of the effects of remedial works (toe buttressing, pumped drainage, gravity drainage, and/or infiltration protection) and long term response of the landslides to external factors such as earthquake, rainfall events and floods (Macfarlane, 2009). In France, the Electricite de France SA (EDF) monitors some potential landslides around a few reservoirs (D. Aelbrecht, pers. comm. 2011). In Mexico, rock-slope problems were investigated for three hydropower projects, including geotechnical investigations, instrumentation, and remedial measures such as drainage systems (Sánchez-Trejo and Espinosa, 1979).

In Canada the British Columbia Hydro and Power Authority (BC Hydro) monitors some slow-moving, deep-seated rockslides in the Columbia River Valley, British Columbia (J. Clague, pers. comm. 2011), notably the Downie Slide with an estimated volume of 1.5 billion m³, making it the largest active slope instability in the world (Kalenchuk et al., 2012). The Downie slide is located 66 km upstream from the Revelstoke Dam (flooding the river past the Downie slide area) and 83 km downstream from the Mica Dam. The major investigation that was initiated in 1965 involved both evaluating factors which could have influenced the initial sliding and assessing the possibility of future hazards due to slide reactivation (Piteau et al., 1978). Drainage measures to lower the piezometric pressures at the Downie Slide below the effect of the reservoir are described by Imrie et al. (1991). Enegren and Imrie (1996) discuss the level of effort and expenses required for monitoring of slope deformations and piezometric levels as well as for

Table 3

Full-scale “rockslide box” parameter values used in the 2D laboratory experiments by Sælevik et al. (2009). To ease the comparison with the scenarios applied for the hazard zoning (Table 2), the volume estimates are here based on a doubled box width of 450 m (corresponding to 0.90 m in laboratory scale, as used in the 3D laboratory experiments).

Scenario	Height [m]	Length [m]	Impact velocity [m/s]	Volume [10 ⁶ m ³]
S1	80	1000	54.8	36
S2	80	500	75.6	18
S3	60	800	79.6	21.6

maintaining the draining measures, early-warning systems, etc., of a large rockslide. An overview of the extensive work on monitoring, hazard analysis, and mitigation of the Downie Slide is presented by Kalenchuk et al. (2012). The BC Hydro rockslide tsunami risk management programme is briefly discussed by Lawrence et al. (2013).

In the United States, a rock wedge failed above the abutment of the Libby Dam during construction in 1971. This caused concern about the stability of the areas in the vicinity of the dam. Potential for sliding had previously been seen with recognition of prehistoric slides and another small wedge slide in 1967. Hence, the possibility of large rockslides and tsunamis were thoroughly investigated, potential rockslide zones were drained, and the slopes were monitored and locally reinforced (Galster, 1991; Voight, 1979).

The analyses related to the Downie Slide (Chaudhry et al., 1983; Kalenchuk et al., 2012), the Mica Dam (Ball, 1970; Slingerland and Voight, 1979) and the Libby Dam (Davidson and McCartney, 1975; Davidson and Whalin, 1974; Raney and Butler, 1976; Slingerland and Voight, 1979; Voight, 1979) demonstrate how establishment of hydro-power reservoirs have initiated a series of pioneering laboratory experiments and development of numerical models and thus substantially increased the understanding of rockslide tsunamis. Laboratory experiments on reservoir rockslide or snow avalanche tsunamis were performed also in Norway at an early stage (Eie et al., 1971; NHL, 1983; VHL, 1967). Field-scale experiments releasing rockslide volumes of 120 000 m³ and 50 000 m³ as well as rock falls of 2000–20 000 m³ into lake Årdalsvatn were performed already in 1969 (VHL, 1969). Water surface elevations and run-up heights were measured along the lake. A dam is constructed by the lake to protect the village Øvre Årdal from tsunamis.

Other studies related to rockslide tsunamis that should be mentioned are in the first place the analytical solutions developed by Noda (1970), partly based on the experimental results by Wiegel et al. (1970). These were succeeded by laboratory experiments by Kamphuis and Bowering (1970), Huber (1982), Huber and Hager (1997), Fritz (2002), Fritz et al. (2003a, 2003b, 2004), and Zweifel et al. (2006). Rockslide tsunami heights are further predicted by empirical models (e.g., Ataie-Ashtiani and Malek-Mohammadi, 2006; Slingerland and Voight, 1979). Mader (1999, 2004) presents numerical simulations of the 1958 Lituya Bay event that agree well with both the field observations and the experimental results by Fritz et al. (2001), see also Fritz et al. (2009) and Weiss et al. (2009). Pastor et al. (2009) present numerical modelling of fluidization processes on fast landslides by pore pressure generation, and their effects in terms of wave generation (again with example calculations for the 1958 Lituya Bay event). The three-dimensional multiple-fluid numerical model by Abadie et al. (2010) reproduces earlier laboratory experiments including the deformable granular flows studied by Fritz (2002). Riemer (1995) discusses the possible impacts of landslides on reservoirs with a review of case histories and methods for hazard and risk assessment as well as risk reduction. Strategies for reservoir landslide investigation and monitoring, modelling (of both landslide and tsunami), and risk management and mitigation are summarized by ICOLD (2002). The status of laboratory experiments and numerical modelling of rockslide tsunamis is summarized by NGI (2004a).

The French RATCOM (Réseau d'Alerte aux risques Tsunamis et submersions CÔtières en Méditerranée) project (<http://meetingorganizer.copernicus.org/EGU2011/EGU2011-14189.pdf>) is meant for early detection and rapid warning of near-field tsunamis caused by earthquakes or submarine landslides in the Ligurian Sea. However, the system is based on a comparison between seismological and (coastal) oceanographic data with pre-computed scenarios to assess the acute tsunami threat, which might make it too time-consuming for rapid warning. Nor is tsunami warning based on seismic signals combined with deep water pressure sensors transmitting signals to warning centres via surface buoys and satellites (again based on comparison with pre-computed scenarios; used among others by NOAA and UNESCO-IOC for oceanic earthquake tsunami warning) applicable or sufficient in fjords or lakes. This is partly because of another source mechanism

and partly because of the short travel time of the tsunami from the rockslide area to the risk-prone areas.

Bellotti et al. (2009) discuss rapid tsunami early-warning systems for small volcanic islands exposed to landslides at the coast of the island itself. They conclude that an efficient system should include offshore wave gauges as offshore waves propagate faster than waves in shallower coastal waters (enabling earlier detection). They further state that pressure disturbances at the bottom are hardly detectable using standard pressure sensors (the waves propagating offshore are considered deep water waves at a small distance from the island, this contradicts the Åkerneset rockslide tsunamis in Storfjorden), and that wave dispersion leaves more time for warning than first expected (maximum inundation occurs later than first arrival).

Finally, it should be noted that the tsunami studies for Åkerneset/Storfjorden are comprehensive, but by far not the only analytical/numerical rockslide tsunami studies in Norway. Other such studies comprise firstly back-calculations of the 1934 Tafjord, Norddal, and the 1983 Årdalstangen, Årdal, fjord tsunami events (Harbitz et al., 1993; NGI, 1984). Further, impact analysis for rockslide tsunamis in fjords are performed for Sørfjorden, Hyllestad (Harbitz et al., 2001; NGI, 1999a), Fedafjorden, Kvinesdal (NGI, 2006a), Romsdalsfjorden, Møre & Romsdal County (Hermanns et al., 2013b; NGI, 2002, 2005, 2013d), Lyngen, Troms County (NGI, 2008d, 2010c, 2013c), and Aurlandsfjorden, Aurland (NGI, 2009). Impact analysis for rockslide tsunamis are also performed for the lake Vassbygdevatn, Aurland (Harbitz, 1988; NGI, 1989), and for the hydropower reservoirs Osavatnet, Osterøy (NGI, 1999b), Mysevatnet, Kvinnherad (NGI, 2003b), and Zakariasvatnet, Norddal (NGI, 2004b); see also (Furseth, 2012; Harbitz et al., 2009).

2. Rock-slope stability and rockslide scenarios at Åkerneset and Hegguraksla

The main aim of the geoscientific investigations of Åkerneset and Hegguraksla rock slopes has been to establish the geological constraints in terms of structural pattern, geomorphic features, geometry, depth of unstable areas, water conditions, and the movement pattern both on the surface and at depth. The investigations have included geological, geophysical, and kinematic studies (Blikra, 2012; Derron et al., 2005). More specifically, the investigations of the Åkerneset rock slope included field mapping, geophysical surveys (resistivity, ground-penetrating radar, seismic), diamond-drilled boreholes, in-borehole logging, laboratory testing of rock samples, LiDAR laser measurements, and tracer tests (ground water flow). At the Hegguraksla rock slope, field mapping and LiDAR measurements have been carried out.

The Åkerneset rock slope (Fig. 4) consists of biotitic, granitic, and dioritic gneisses. Three distinct fracture sets were identified by Ganerød et al. (2008): fractures parallel to the foliation, fractures roughly normal to foliation trending N–S, and fractures roughly normal to foliation trending E–W. The fracture set parallel to the foliation is sub-parallel to the slope, and these fractures with dip angle about 35° are the main reason for the instability of the Åkerneset rock slope. The upper instability at Hegguraksla consists of a 250-m-high column of two rock types: orthogneiss in the lower part and augengneiss in the upper part. A large open NNE–SSW-trending fracture acts as tension crack. The lower instability consists of gneiss and is characterized by a large opening along the back-crack in the northern part of the instability (Oppikofer, 2010).

The Åkerneset rock slope is monitored by rod extensometers, differential GPS, instrumented boreholes, two single lasers for distance measurements across the uppermost extension cracks, periodic laser scanning (ground-based LiDAR), in summertime a LISALab ground-based Interferometric Synthetic Aperture Radar (INSAR), satellite-based radar, a seismic network of geophones, an automated total station with 30 prisms, a weather station, and web cameras (ÅTB, 2010a; Blikra, 2012). High-resolution topographic data were obtained from an airborne LiDAR campaign. The displacements recorded 900 m.a.s.l. (in the upper part of the possible Åkerneset rockslide) are about 15 cm/year

in the western end and a few cm/year in the eastern end of the fractures. The Hegguraksla rock slope is monitored by crackmeters, tiltmeters, and a ground-based radar system (ÅTB, 2010b). Displacements of a few mm/year have been indicated at the upper instability by the measurements that started in December 2008.

Two failure scenarios for each of the two unstable rock slopes are applied for the hazard zoning, see Fig. 3 for the locations and Table 2 for the scenario parameters (further described by ÅTB, 2011; NGI, 2014). The maximum credible worst-case volume of the potential Åkerneset rockslide is estimated to 54 Mm³. This corresponds to scenario (1C) and comprises approximately the whole shaded area in Fig. 4. The western flank scenario (2B) is estimated to a volume of 18 Mm³ that comprises the upper part of the shaded area (Fig. 4; Kveldsvik et al., 2009; L.H. Blikra, pers. comm. 2012). Geological findings in the Åkerneset rock slope confirm that simultaneous releases of large blocks or even the total volumes (Fig. 4) are not unlikely. The impact velocity for both scenarios is estimated to 45 m/s (NGI, 2014). The further velocity progression of the rockslides (and hence the run-out distance) applied in the calculations mimics the observations from the laboratory experiments (Fig. 5). It should be noted that the Åkerneset rockslides continue to accelerate after impact with the water surface until they reach the approximately horizontal bottom. The temporary deceleration of the rockslide during impact with the water is of minor importance for the rockslide progression (NGI, 2014).

The two scenarios from the upper part of the Hegguraksla rock slope comprise 2 Mm³ (H2) and 3.5 Mm³ (H3), respectively, both with an estimated impact velocity of 60 m/s (calculated by the PCM block model, Perla et al., 1980). For the scenarios from the Hegguraksla rock slope, the subaqueous rockslide velocity is estimated from a prescribed velocity function and a run-out distance of 750 m (approximately midfjord) determined from bathymetric evaluations and mapped deposits of ancient events (NGI, 2003a). The nominal probability is considered between 1 in 1000 and 1 in 5000 years for scenarios 1C and H3, and larger than 1 in 1000 years for scenarios 2B and H2, Table 2 (ÅTB, 2011). The largest uncertainty in the numerical results is related to the release process and the configuration of the rockslide elements entering the water in a real event. In the calculations, the rockslides are implemented as “rounded boxes” that represent the worst case (simultaneous release) for each individual volume.

The characteristic seabed plain of the fjords results primarily from glacial erosion widening narrow valleys while also steepening the lateral slopes due to higher shear stresses and erosion on the sides. Subsequently, the broader valleys are deepened due to thicker ice and higher bed temperatures that enable slip conditions with higher velocities, both promoting enhanced erosion along the bed (thus a self-reinforcing effect). The subsequent sedimentation has levelled the fjord bottom with layers typically thicker than 100 m (C.F. Forsberg, O.A. Høydal, pers. comm. 2012; Vorren and Mangerud, 2008). Outside Åkerneset, the seabed sediments are up to 180 m thick. On top is a 4 m thick layer of soft silty clay (perhaps a bit more arenaceous on the surface) that will form the bed beneath a possible rockslide (NGU, 2009a; O. Longva, pers. comm. 2012).

3. Laboratory experiments

Laboratory experiments were accomplished in the two-dimensional (2D) wave channel at the Hydrodynamics Laboratory, University of Oslo (the channel wave generation area is shown in Fig. 6), and in the three-dimensional (3D) 1:500-scale model at the SINTEF Coast and Harbour Research Laboratory (SINTEF, 2008). NGI (2014)² discusses the

² NGI (2014) recommended a front angle of 30° (probably not more than 45° and not less than 15°) relative to the glide plane. In the 2D experiments, a front angle of 45° was applied as a worst-case approach. In the 3D experiments, the front of the slide was perpendicular to the glide plane (A. Lothe, pers. comm., 2008).

configuration, dimensions, and velocity progression to be used for the laboratory “rockslide box”.

The model used in the 2D experiments was a 1:500 geometrically scaled cross section of the fjord outside the Åkerneset rockslide area. The dimensions of the wave channel constrained the box width to a fixed value of 0.45 m. Seven different scenarios (including scenario 2B) were conducted to cover a reasonable range of parameter value combinations. These scenarios (together with other factors such as likelihood) were also later looked to when establishing the two Åkerneset rockslide scenarios 2B and 1C applied for the hazard zoning (ÅTB, 2011). The set-up and results of the 2D experiments are reported by Jensen et al. (2007). Three of the seven scenarios were studied in more detail by Sælevik et al. (2009), admittedly with somewhat larger impact velocities than applied by Jensen et al. (2007). The full-scale parameter values of these three rockslide scenarios S1–S3 are presented in Table 3 (unfortunately, none of these three scenarios corresponds directly to the scenarios later adopted for the hazard zoning). The surface elevations at three locations outside the impact area were measured with non-intrusive ultra-sonic wave gauges. In addition, velocities were measured using Particle Image Velocimetry (PIV). Sælevik et al. (2009) further investigated the effects of rockslide volume and length. They concluded that the rockslide volume was the governing parameter for the height of the leading wave, and that the length of the rockslide box seemed to be more important for the trailing wave in the three scenarios S1–S3. Shorter rockslide boxes (e.g., scenario S2) provided a deeper cavity favouring an earlier collapse of the leading wave and a higher trailing wave than observed for the longer boxes (scenario S1). Finally, they concluded that the height of the rockslide box did not give any notable change of the waves generated from the impact. Valuable experience on the functionality and location of the monitoring devices was transmitted to the 3D experiments.

The 3D model covers the inner part of Storfjorden (Sunnlyvsfjorden and Geirangerfjorden), Fig. 7. At the northern boundary ($y = 6900$ km) a wave damper extracts the energy to avoid false reflections. The 3D experiments were performed later than the 2D ones. At that time, a need

to study larger volumes was realized. Hence, three of the scenarios used in the 2D experiments were replaced by larger volumes in the 3D experiments. The design, the seven scenarios (now including both 2B and 1C), the setup, and the results of the 3D experiments are described by SINTEF (2008). The twelve gauges depicted in Fig. 7 measure the surface elevations using resistive wave sensors. In addition two level sensors measuring the water level are located in the run-up zones at Hellesylt (coordinates in UTM32: 389092 m, 6885273 m) and Geiranger (406234 m, 6886498 m). Finally, the particle velocity at three gauges (positioned just SW of the corresponding surface elevation gauges 4, 5, 6) is logged during each experiment. The results of the 3D experiments were applied as input to and validation of the numerical models (Section 4.3.2).

4. Numerical modelling

4.1. Digital elevation models

For the outer part of Storfjorden (Fig. 3), the applied bathymetry is based on the best available data from the Norwegian Hydrographic Service, while for the inner part both the bathymetry and the topography are based on data with resolutions of 3 m (in shallow water areas) and 6 m. All the data are provided by the Norwegian Geological Survey (NGU), and interpolated onto a uniform grid with a resolution of 50 m for calculations of tsunami propagation, and onto grids with resolution ranging from 5 m to 40 m (depending on nested grid level) for calculations of tsunami run-up.

For the hazard zoning, the topography in the inundation zones (except for Hellesylt) is based on data provided by The County Governor of Møre & Romsdal. The original data used in the run-up calculations are high-resolution 1 m contour lines including the shoreline. For Hellesylt, the data from NGU (described above) with a resolution of 5 m (raster data with a better representation of the topographic details in the valley south of Hellesylt) are applied for the run-up calculations. The topography and bathymetry applied for the run-up calculations are filtered in a

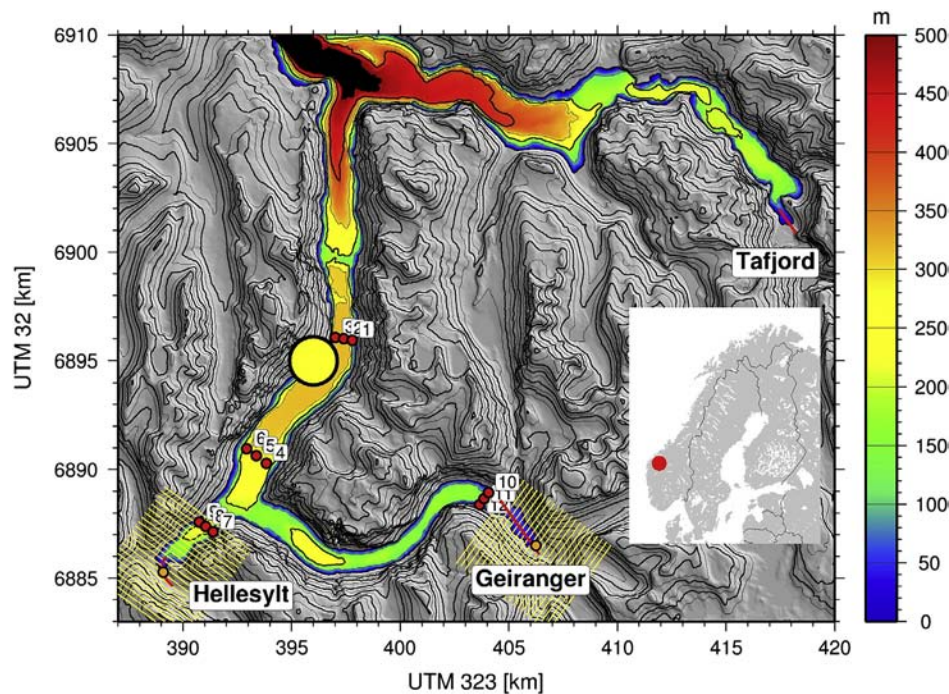


Fig. 7. Bathymetry and topography data constituting the basis for the 1:500-scale laboratory model. The bigger yellow bullet indicates the location of the potential rockslide at Åkerneset. The red bullets (numbered 1 to 12) are the gauges where the surface elevation is measured. The two smaller orange red dots show the location of the run-up height measurements in both the laboratory experiments and the numerical modelling. The yellow lines indicate the tracks for the transverse depth profiles (with 250 m in between) used to establish the reconstructed bathymetry for the run-up calculations at Hellesylt and Geiranger, which is then identical to the 1:500-scale laboratory model. The red lines indicate the location of the longitudinal transects in Figs. 12 and 22. (For interpretation of the references to colour in this figure legend, the reader is referred to the web version of this article.)

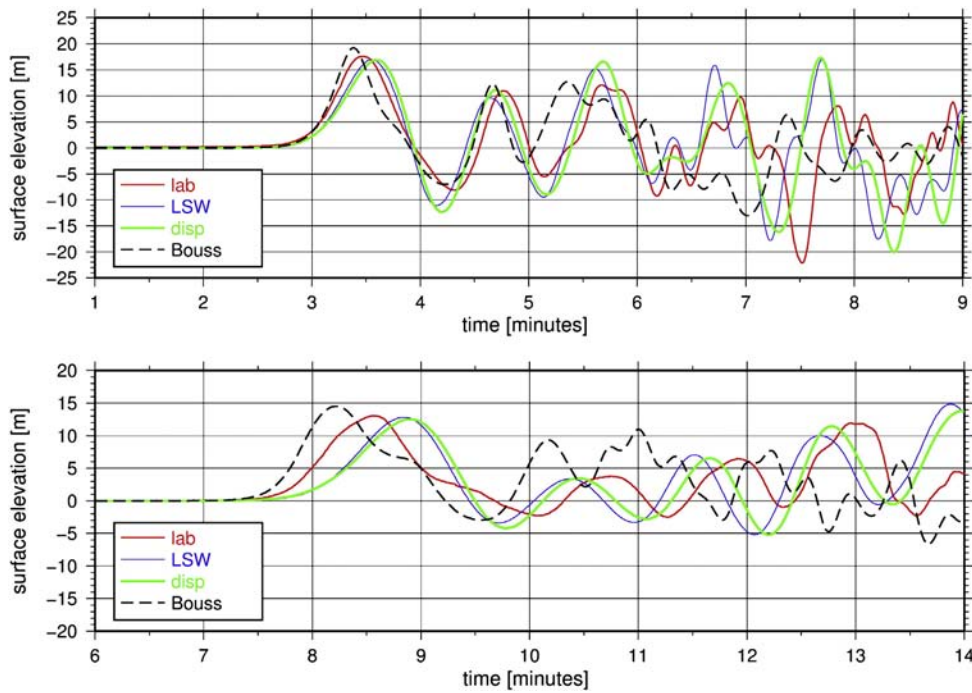


Fig. 8. Comparison of laboratory and numerical results with input from laboratory experiments at gauge 4–6 using scenario 1C (nominal probability between 1 in 1000 and 1 in 5000 years). The figure shows results at the gauges 8 (outside Hellsylt, upper panel) and 11 (outside Geiranger, lower panel). “lab” is the surface elevation measured in the laboratory, while the other keys refer to different mathematical descriptions in the numerical model: “LSW” – linear shallow water (hydrostatic), “disp” – linear dispersive, and “Bouss” – nonlinear and dispersive.

prescribed zone along the shoreline simply by elevating/lowering points such that the slope is kept below a maximum value. This is made to avoid too high current velocities (in particular during withdrawal) and thus potential numerical instability. Following from the guidelines established by the Norwegian Water Resources and Energy Directorate (NVE), who is responsible for rockslide risk management in Norway, and the instructions from the County Governor of Møre & Romsdal County, an expected sea-level rise due to climate changes is considered. A sea-level rise for the period 2010–2100 of 0.7 m (DSB, 2009) is here taken into account in the calculations for the hazard zoning.

4.2. Computational models

Numerical modelling of rockslide tsunamis in a complex fjord system is a complicated task, and the work is performed via a series of different approaches to improve the final result. The simulations are divided into two stages: open-fjord propagation including the initiation of the waves and near-shore propagation including dry-land inundation. When the wavelengths are not much longer than the water depth, the pressure is no longer hydrostatic and the waves will be influenced by dispersive effects implying that the speed of wave propagation depends on the wavelength. Moreover, if the surface elevation is significant in relation to the water depth, the waves will be nonlinear. This effect can be seen as steepening of waves propagating towards the shore, followed by possible wave breaking. To include dispersion and nonlinearity, numerical models based on the Boussinesq equations are applied for the open fjord propagation. The first model is labelled GloBouss (Løvholt et al., 2008, 2010; Pedersen and Løvholt, 2008), and the second model is labelled DpWaves³ (Langtangen and Pedersen, 1998; NGI, 2008e). Both models have the option of simulating rockslide-generated waves. The rockslide is represented either by a rounded box with prescribed physical dimensions and velocity progression along a

linear or a curved path, or by invoking the output from numerical rockslide models. DpWaves is the only model capable to be initiated by the time-history along a boundary (forced input), and is the model applied for simulating waves with input from the laboratory experiments as described in Section 4.3.2. In all other simulations, we apply the more robust and less computationally demanding GloBouss model.

The nonlinear terms in the Boussinesq models may lead to instability if the seabed is reclaimed during simulation. This problem is especially severe in the generation area, but is also pronounced in more distant shallow areas. The problem is overcome by replacing shallow water depths by a threshold value. This value is linearly and radially decreasing from a minimum water depth of 300 m in the generation area (where we find the largest waves with deeper troughs) to a minimum water depth of 50 m at a distance of 4 km or more away from the generation area. Hence, stable Boussinesq solutions are obtained during the simulations. For comparison between the different mathematical descriptions, the same threshold depth is applied for all simulations regardless of the mathematical description. Since the speed of wave propagation depends on the transverse average depth of the fjord, the waves in the numerical solution will propagate slightly faster than the waves observed in the laboratory experiments.

For near-shore propagation and inundation in selected locations, we apply the MOST model (ComMIT, 2011; Titov, 1997; Titov and Synolakis, 1995, 1998), taking nonlinearities in the shallow-water propagation (including potential wave breaking) into account. By using a one-way nesting procedure, MOST reads the output from the propagation model (GloBouss or DpWaves) over the model boundaries at each time step. This enables a swift one-way nesting of dispersive wave propagation with run-up models (Løvholt et al., 2010).

4.3. Validation of numerical models

4.3.1. Verification and sensitivity tests

The set of applied numerical models is first carefully verified against analytical solutions. Secondly, systematic sensitivity analyses for grid resolution, mathematical wave models, rockslide configuration and

³ Used in “mild-slope” mode to avoid numerical instabilities related to steep depth gradients, see Løvholt and Pedersen (2009).

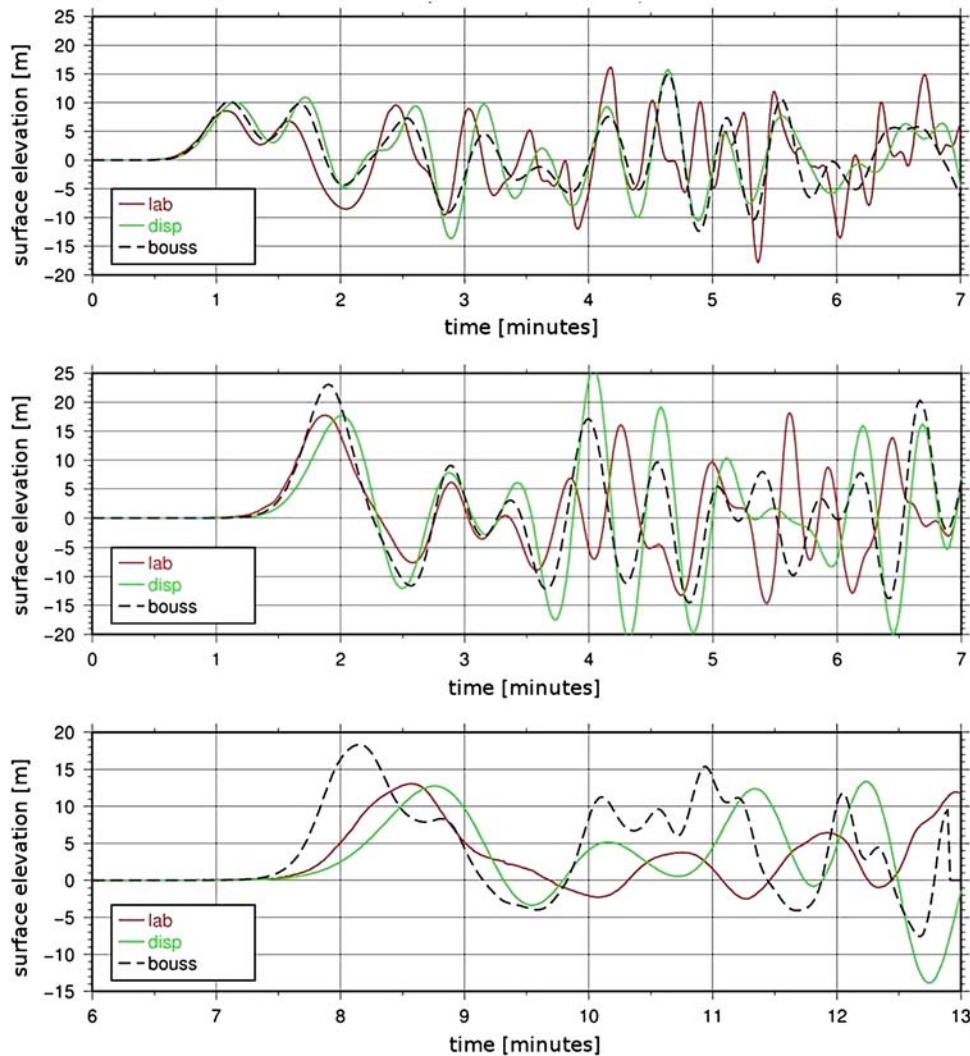


Fig. 9. Surface elevations from laboratory experiments compared to numerical simulations. In this case, the wave generation is modelled numerically. Comparisons for scenario 1C (nominal probability between 1 in 1000 and 1 in 5000 years) at gauges 2 (upper panel), 5 (mid panel), and 11 (lower panel). For explanation of the different keys applied in the figure, see Fig. 8.

dimension, and rockslide dynamics (direction, impact velocity, velocity profile, run-out distance, skin friction), are accomplished. Among other things it is found that dispersion in the generation phase may be crucial. Dispersive models seem to describe the wave generation and propagation remarkably well, while hydrostatic models overestimate the height of the leading wave. The frontal area of the rockslide is more important for wave generation than the impact velocity and the rockslide volume; maximum rockslide velocities of 50 m/s and 70 m/s returned insignificant differences in the run-up heights. A change of the rockslide direction at Åkerneset has stronger influence on the waves propagating northward than southward. The effect of the skin friction at the rockslide/water interface on the generated waves can be neglected. For further details on the sensitivity tests, see NGI (2006b, 2008e).

4.3.2. Validation against laboratory experiments

Numerical results based on Boussinesq theory were compared with the velocities measured in the 2D experiments. The agreement was good after some distance of propagation away from the source area. Interpolated values based on the surface elevation in the 3D experiments measured in gauges 1–3, Fig. 7 (for waves travelling northward) and in gauges 4–6 (for waves travelling southward) together with the corresponding velocity potential (deduced from the surface elevation using the linear hydrostatic relation) are applied as forced input to the numerical DpWaves propagation model along the boundary lines defined by

these gauges. Alternatively, a comparison is made between the laboratory and the numerical results where also the wave generation is simulated numerically (no input from the laboratory experiments to the numerical models). The dimensions and velocity progression of the rockslide are then identical to the ones in the laboratory experiments.⁴ In both cases, the leading waves are fairly well reproduced compared to the laboratory experiments despite a phase-shift of the leading wave for some of the solutions, Figs. 8 and 9. It is evident that there are larger problems with reproducing the trailing waves that are more influenced by nonlinearity, reflections, and run-up along the fjord. These processes may not be accurately captured by the numerical models (Løvholt et al., 2013). However, numerical tests show that even for trailing waves larger than the leading ones, the longer and leading waves heading directly to the fjord heads give the larger run-up, while trailing waves may cause the highest run-up at locations along the fjord. Most of the way the wave period increases with increasing distance of propagation, probably caused by dispersion as well as wave filtering through the bends and divides throughout the fjord system (Harbitz, 1992). Altogether, the best match is found for the larger scenarios (revealing less pronounced scale effects) with the linear

⁴ It should be kept in mind that the frontal angle applied in the numerical modelling is slightly less than 45°, while the front of the slide in the 3D laboratory experiments was perpendicular to the glide plane.

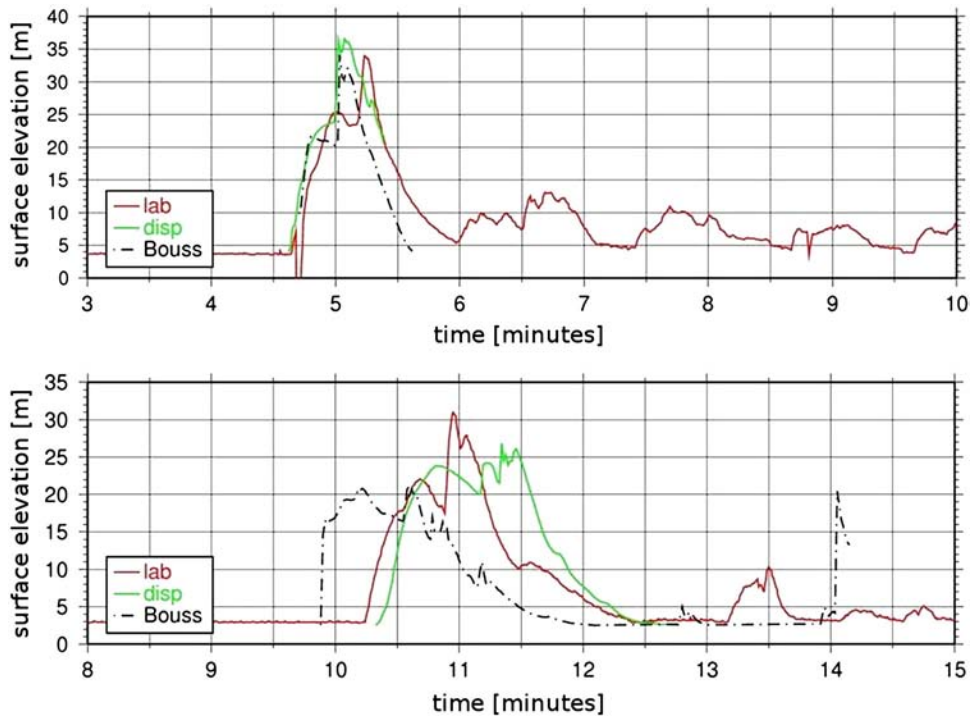


Fig. 10. Comparison between run-up heights for scenario 1C (nominal probability between 1 in 1000 and 1 in 5000 years) from the laboratory experiments and from the numerical simulations with input from the laboratory experiments at Hellesylt (upper panel) and Geiranger (lower panel). For explanation of the applied keys, see Fig. 8. The locations for the run-up height measurements are shown in Fig. 7.

dispersive solution for the propagation phase (as nonlinearity steepens and amplifies the leading wave in the larger scenarios more in the numerical solutions than in the laboratory experiments, Fig. 8). The Boussinesq solutions overestimate the laboratory experiments more and more with distance from the rockslide area, and a solitary wave is presumably formed (Fig. 8 upper panel, Fig. 9 lower panel). The

discrepancies between the numerical solutions and the laboratory experiments may also largely be related to the effect of the threshold depth applied in the numerical model.

Results for the corresponding run-up calculations are shown in Figs. 10 and 11. It should be noted that the 1:500-scale model is constructed by linear interpolation between transverse depth profiles

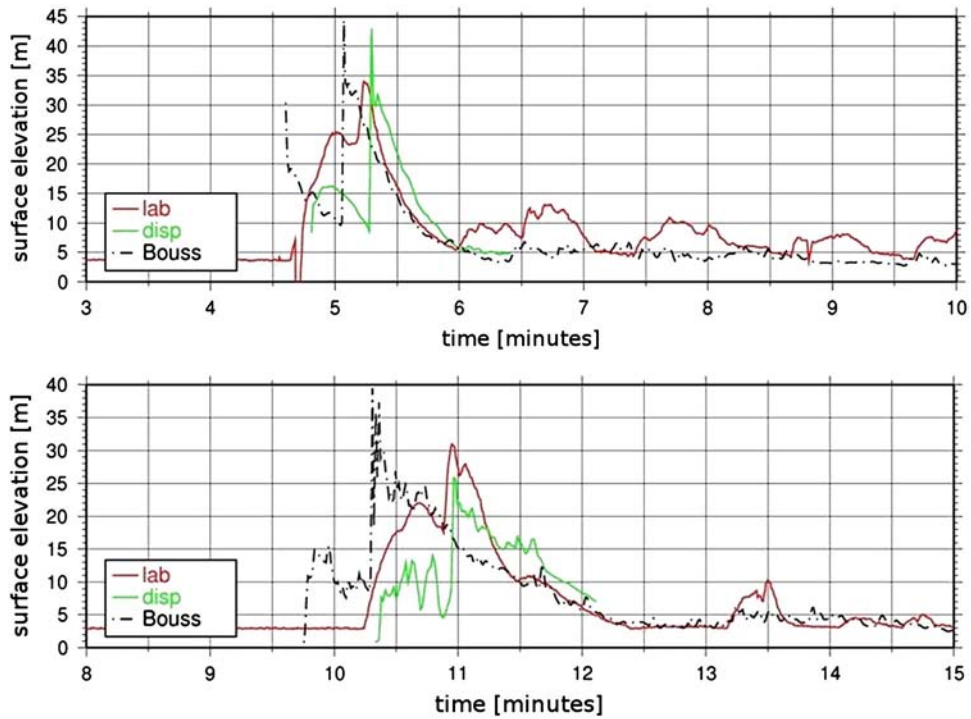


Fig. 11. Comparison between run-up heights for scenario 1C (nominal probability between 1 in 1000 and 1 in 5000 years) from the laboratory experiments and from the numerical simulations with the generation phase modelled numerically at Hellesylt (upper panel) and Geiranger (lower panel). For explanation of the applied keys, see Fig. 8. The locations for the run-up height measurements are shown in Fig. 7.

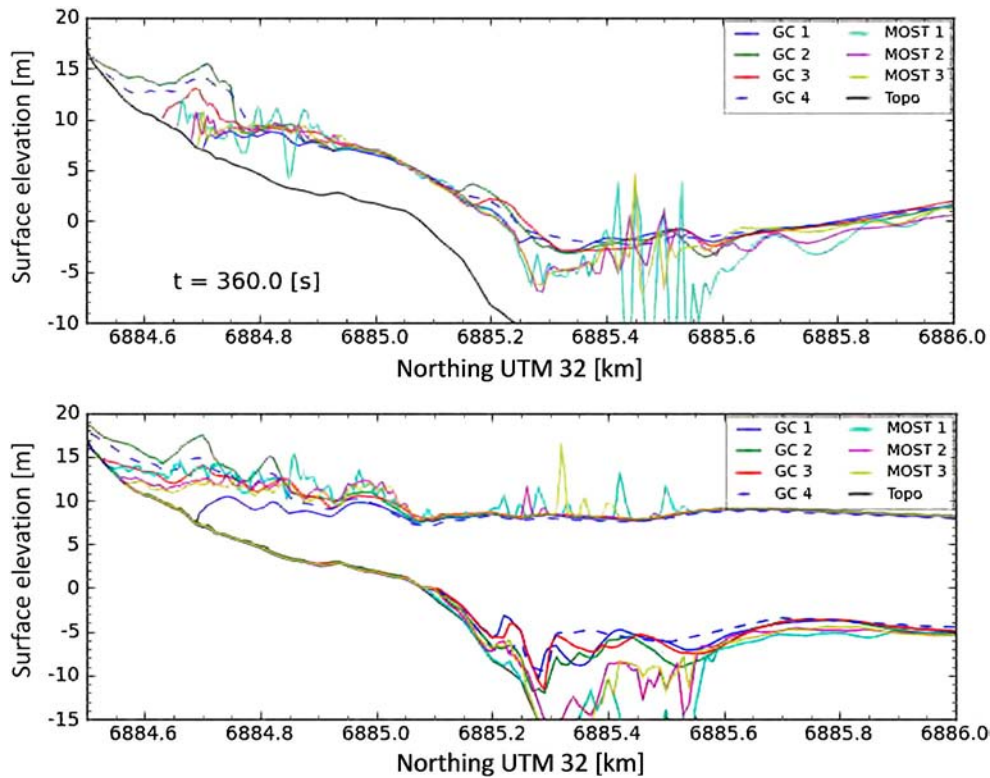


Fig. 12. Inundation heights (together with maximum and minimum surface elevation in the fjord) for the run-up models MOST and GEOCLAW (GC) along the longitudinal transect for Hellesylt shown in Fig. 7. Snapshot after 360 s (upper panel) together with maximum and minimum values during the total computational time of 460 s (lower panel) are shown for a 42 Mm³ rockslide with an impact velocity of 45 m/s. The seven runs can be briefly summarized and evaluated as follows: GC 1 – higher dry tolerance, loses water; GC 2 – highest run-up due to no friction; GC 3 – default friction value, most reliable GEOCLAW simulation; GC 4 – parameter values as in GC 2, but with a first order numerical scheme that did not capture the bore shape; MOST 1 – significantly reduced friction compensating for water loss; MOST 2 – slightly lowered friction, unphysical oscillations and ripples; MOST 3 – default friction value, ripples, fairly limited oscillations. The topography is shown as a full drawn black line. Modified from figures produced by R.E. Bredesen (presented in NGI, 2010a, Appendix B).

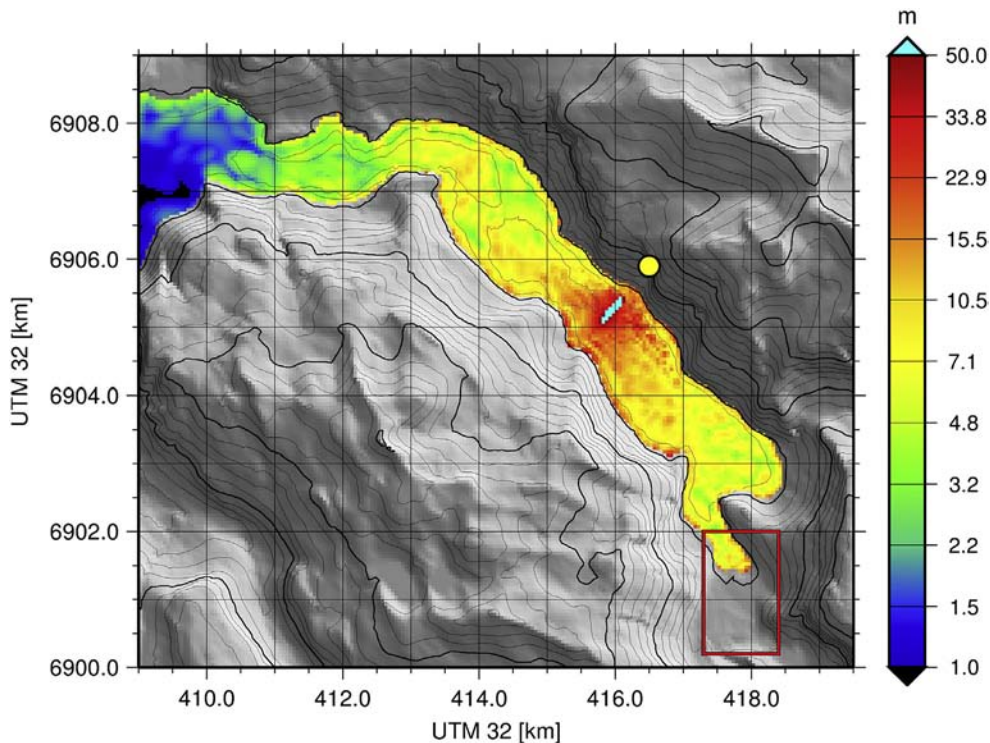


Fig. 13. The maximum surface elevation from the back-calculation of the 1934 Tafjord rockslide tsunami. The rockslide release area is marked with a yellow bullet. The red rectangle is the area for the flow depth calculations at Tafjord village (Fig. 14). (For interpretation of the references to colour in this figure legend, the reader is referred to the web version of this article.)

with 250 m in between (SINTEF, 2008). To reproduce this bathymetry for the numerical run-up modelling, the same procedure was followed as close as possible to establish the digital bathymetry used for run-up model validation at Hellesylt and Geiranger, Fig. 7. Altogether, the discrepancies between the numerical solutions and the laboratory experiments are remarkably small.

Applying interpolated gauge values as input to the nonlinear (Boussinesq) propagation solution, which is subsequently applied as input to the MOST run-up model, somewhat underestimates the run-up height at Geiranger. This may be due to the steeper front of the leading wave for the propagation phase, leading to stronger breaking and reduced surface elevation in the run-up stage. For smaller scenarios, larger

deviations are found (for both Hellesylt and Geiranger), probably due to scale effects (viscosity, surface tension). This contradicts the results by Fritz (2002) who discusses viscous effects, surface-tension effects, and compressibility effects in relation to a 0.5 m wide, 1 m deep, and 15 m long channel and finds that scale effects are negligible. Hence, he concludes that the whole process including granular-slide motion, slide impact, energy dissipation, wave generation, wave propagation, and breaking primarily obey the generalized Froude similitude at the scale of his experimental series.

By modelling the generation numerically, and using the linear dispersive propagation solution as input to the MOST run-up model, the calculated leading wave run-up heights deviate with -5% to $+25\%$

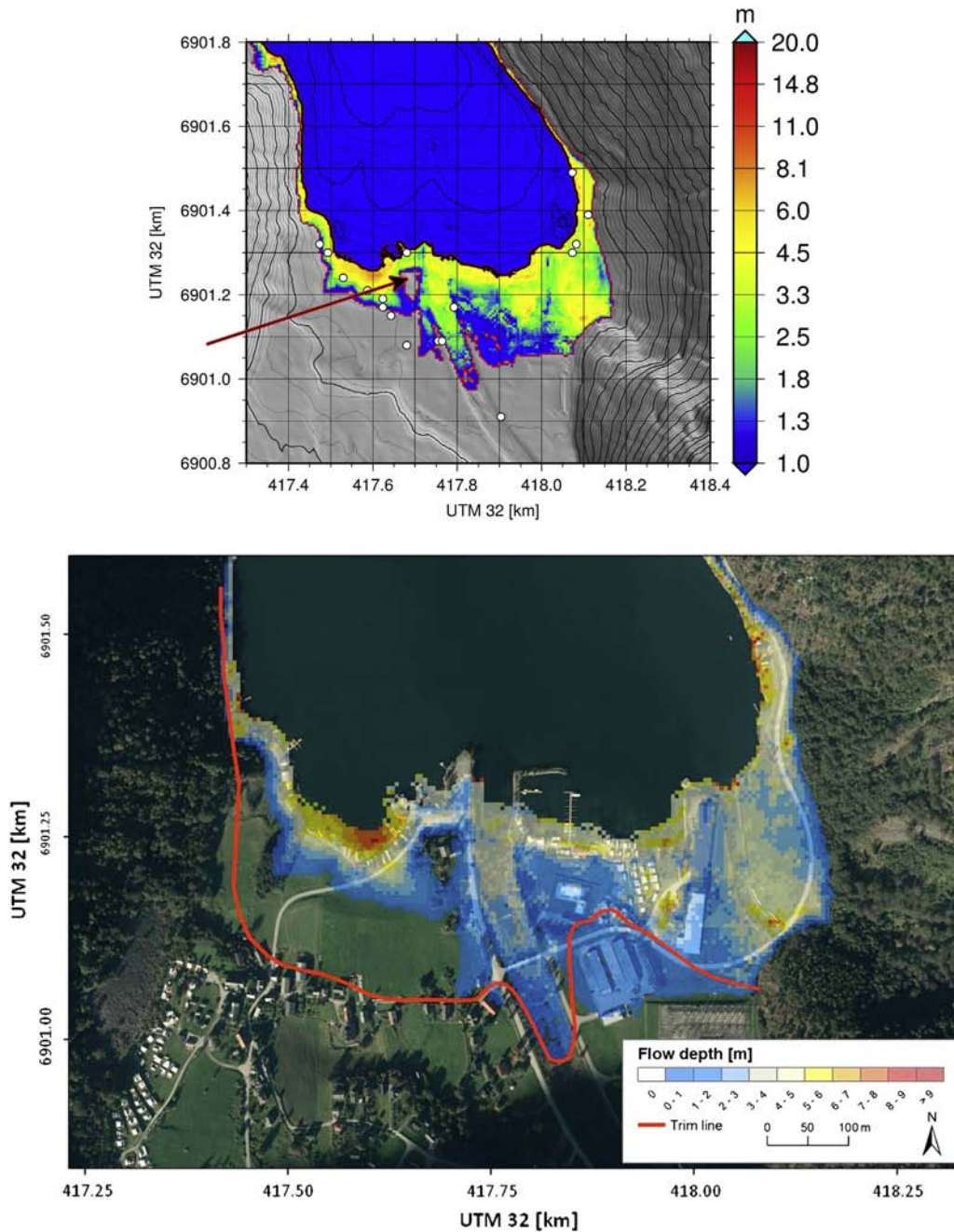


Fig. 14. Maximum flow depth during inundation at the village Tafjord from the back-calculation of the 1934 Tafjord rockslide tsunami. The stone Haugsteinen (see Fig. 2) is seen as an isolated dry spot to the west of the river (at UTM 32 0417679–6901232, indicated by the arrow). Upper panel: Computational domain given by the red rectangle in Fig. 13. White bullets depict the locations where the maximum inundation and run-up heights were measured (the locations are visually deduced by enlarging a figure presented by Jørstad (1968), the corresponding heights are shown as blue stars in Fig. 15). Lower panel: Maximum flow depth overlaid on current terrain (map basis: Norwegian Mapping Authority, Geovekst and municipalities – Geodata AS) and compared to observed inundation distance shown by red trimline (from Furseth, 1985). (For interpretation of the references to colour in this figure legend, the reader is referred to the web version of this article.)

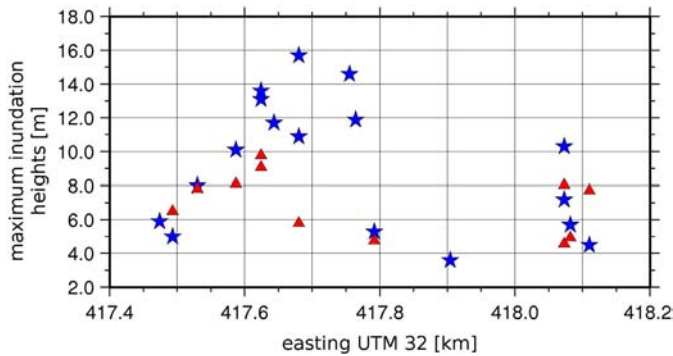


Fig. 15. Comparison between observed (blue stars, from Jørstad, 1968) and back-calculated (red triangles) maximum inundation and run-up heights at the locations in Tafjord shown in Fig. 14 upper panel. (For interpretation of the references to colour in this figure legend, the reader is referred to the web version of this article.)

for the various scenarios impacting Hellesylt and Geiranger. The overestimated wave height in the propagation phase seems to be counteracted by more intensive wave breaking, especially at Geiranger (see also Lynett et al., 2003).

4.3.3. Validation against other numerical models

The performance of the numerical run-up model MOST is confirmed by validation against another run-up model, GEOCLAW (<http://www.clawpack.org>; George and LeVeque, 2006). Like the MOST model, GEOCLAW is based on the nonlinear shallow water (NLSW) equations and handles bores and wave breaking. The GEOCLAW and MOST models produced relatively similar run-up heights for the test area in Hellesylt, especially with regard to the leading waves, Fig. 12 (for further details, see simulations by R.E. Bredesen presented in NGI, 2010a, Appendix B). After reflection of the leading wave and initiation of the drawdown, water losses decrease the confidence in the MOST model with time. Maximum drawdown is too deep for the MOST model, which could

cause numerical instability. When instability occurs, the calculations are stopped before the solution is destroyed. Fortunately, in these cases the leading wave causes the strongest impact on land. Hence, terminating the simulation during drawdown has no influence on the inundation distance and the maximum values as long as the maximum inundation is reached. All open fjord simulations as well as all near shore and inundation simulations are tested for proper convergence (simulations by R.E. Bredesen et al. presented in NGI, 2010a, Appendix C; NGI, 2010a, Appendix E).

4.3.4. Validation against field observations

Finally, three historical events, 1731 Skafjell, 1756 Tjelle, and 1934 Tafjord, are closely reproduced by the numerical GloBouss and MOST models (for summaries of the historical events and previous studies, see Furseth, 2006, 2009, 2012; Harbitz et al., 1993; Jørstad, 1968; NGI, 2010a and references therein). Figs. 13–15 show maximum surface elevation (offshore water level above equilibrium), maximum flow depth (water level above terrain surface), as well as maximum inundation heights (water level above equilibrium at any place in the inundation zone) and run-up heights for the 1934 Tafjord event. The isolated dry spot to the west of the river in Fig. 14 corresponds remarkably well to the location where six persons saved their lives standing on the stone Haugsteinen (Fig. 2), which is about 12 m higher than the contemporary sea level (Furseth, 2009, pers. comm. 2012). By tuning the rockslide parameters, it should be possible to improve the results even further. Based on the comparisons between field-observed and modelled inundation heights and run-up heights for the historical events, it is concluded that the numerical modelling is performed with high accuracy.

5. Main results for the tsunami hazard zoning

This section focuses on results for practical applications in land-use planning and design with regard to rockslide tsunami impact in Storfjorden. There are several ways to quantify the tsunami impact: inundation height, maximum values of shoreline water level, flow depth, current speed, acceleration in the flow direction, momentum, or

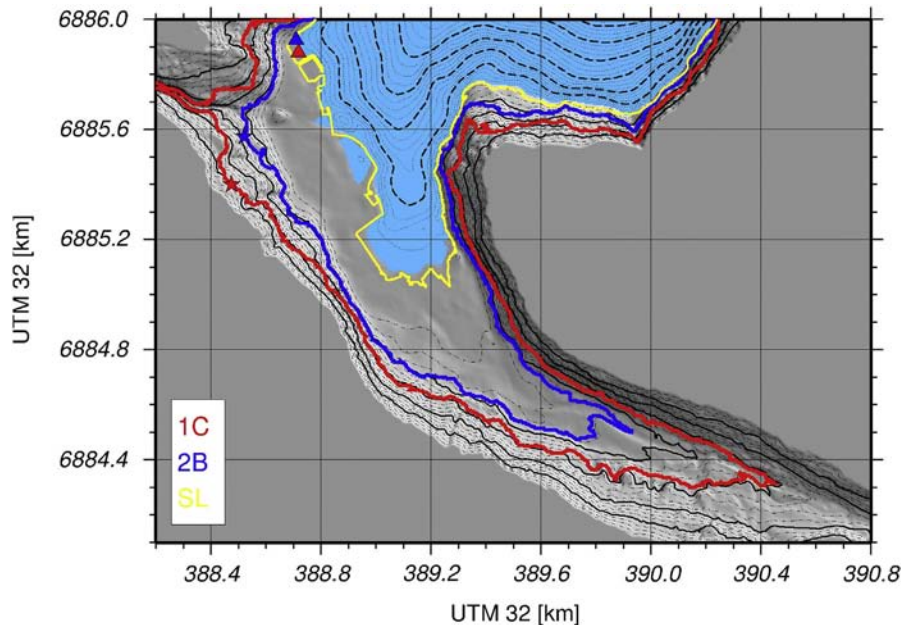


Fig. 16. Trimlines for scenarios 1C (nominal probability between 1 in 1000 and 1 in 5000 years) and 2B (nominal probability larger than 1 in 1000 years) at Hellesylt. The maximum value of the water level along current shoreline and the maximum run-up height are indicated by a triangle and a star, respectively. The heights include the effect of a sea-level rise of 0.7 m. The yellow line is the shoreline for current mean sea level. Contour lines are printed every 200 m. (For interpretation of the references to colour in this figure legend, the reader is referred to the web version of this article.)

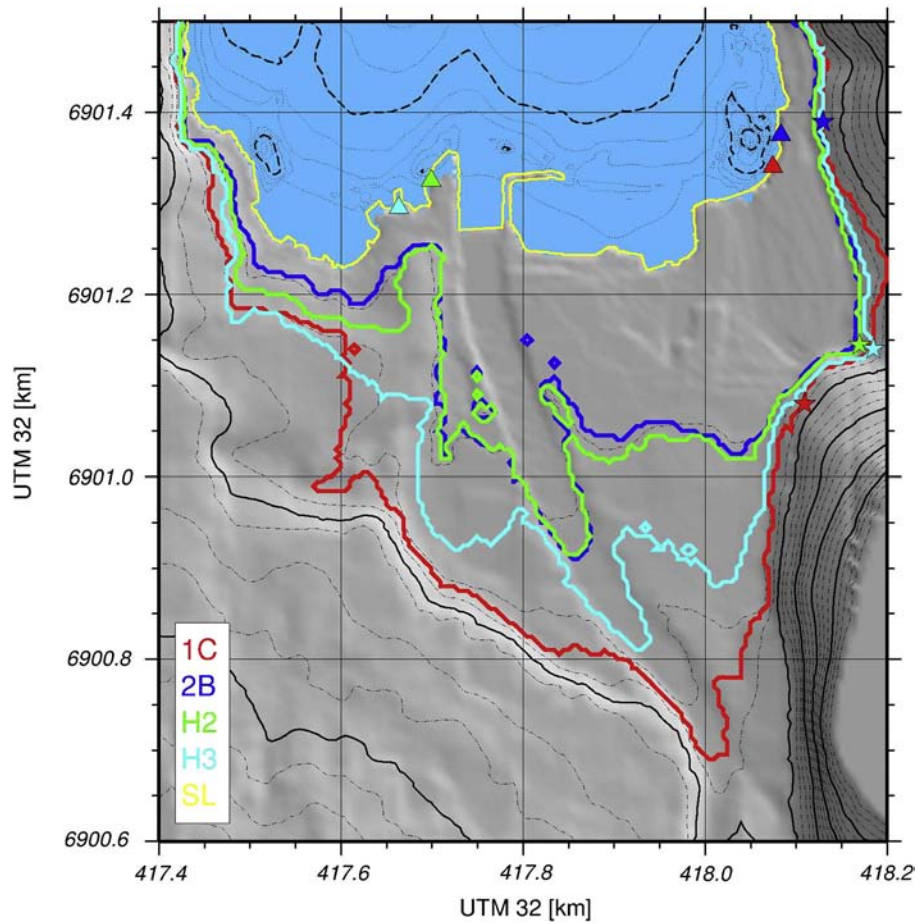


Fig. 17. Trimlines for scenarios 1C, 2B, H2, and H3 at Tafjord (scenario probabilities are presented in Table 2). The maximum value of the water level along current shoreline and the maximum run-up height are indicated by a triangle and a star, respectively. The heights include the effect of a sea-level rise of 0.7 m. The yellow line is the shoreline for current mean sea level. Contour lines are printed every 200 m. (For interpretation of the references to colour in this figure legend, the reader is referred to the web version of this article.)

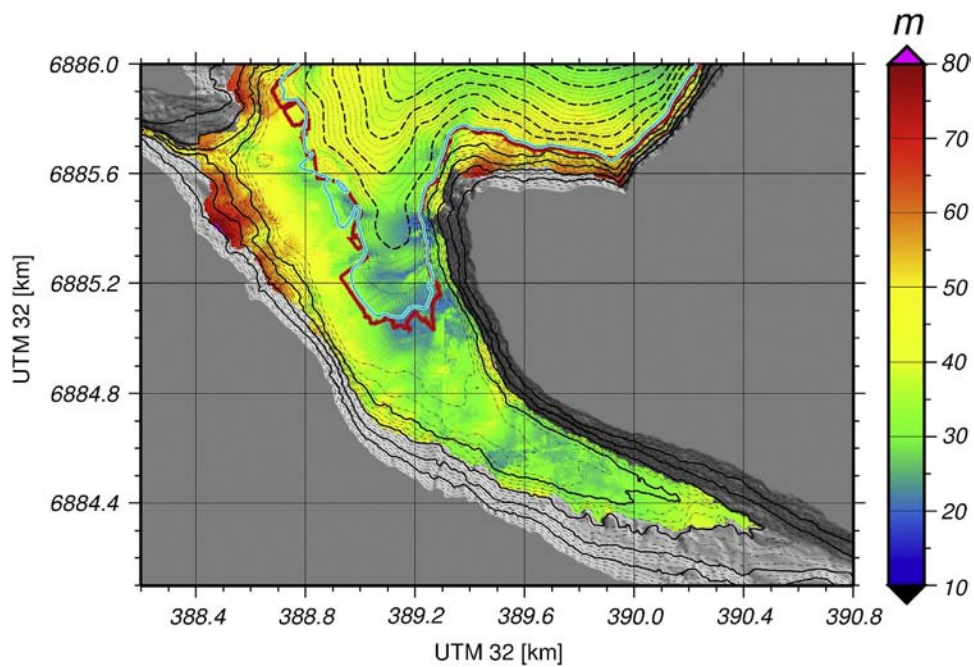
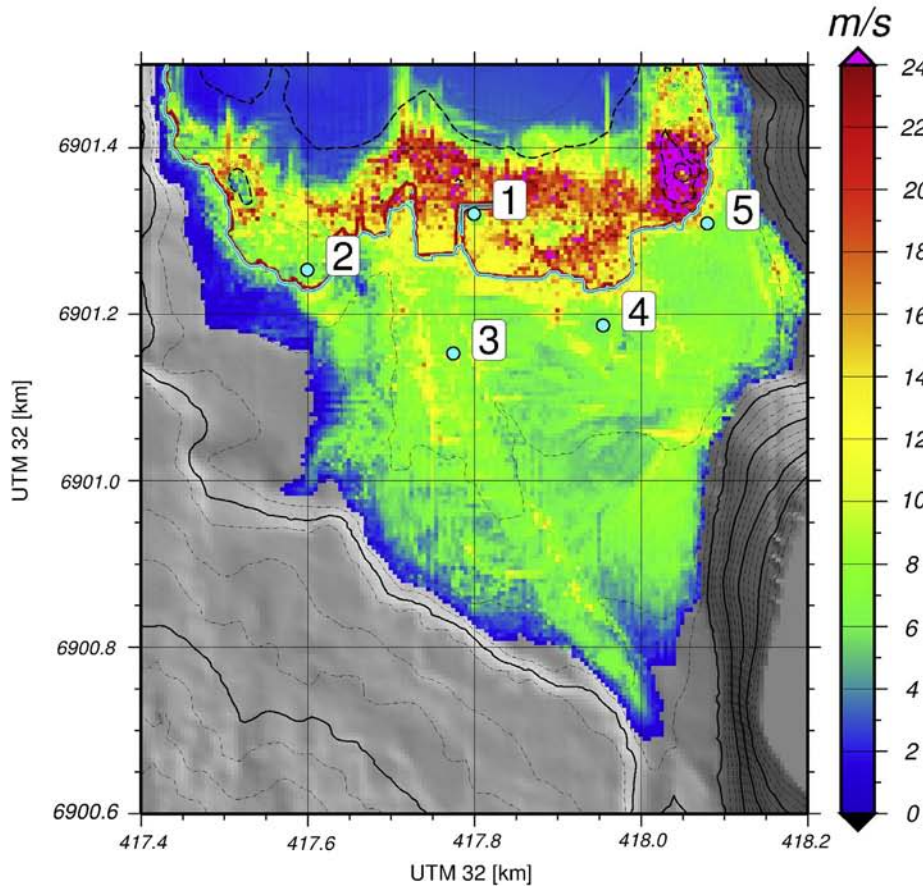
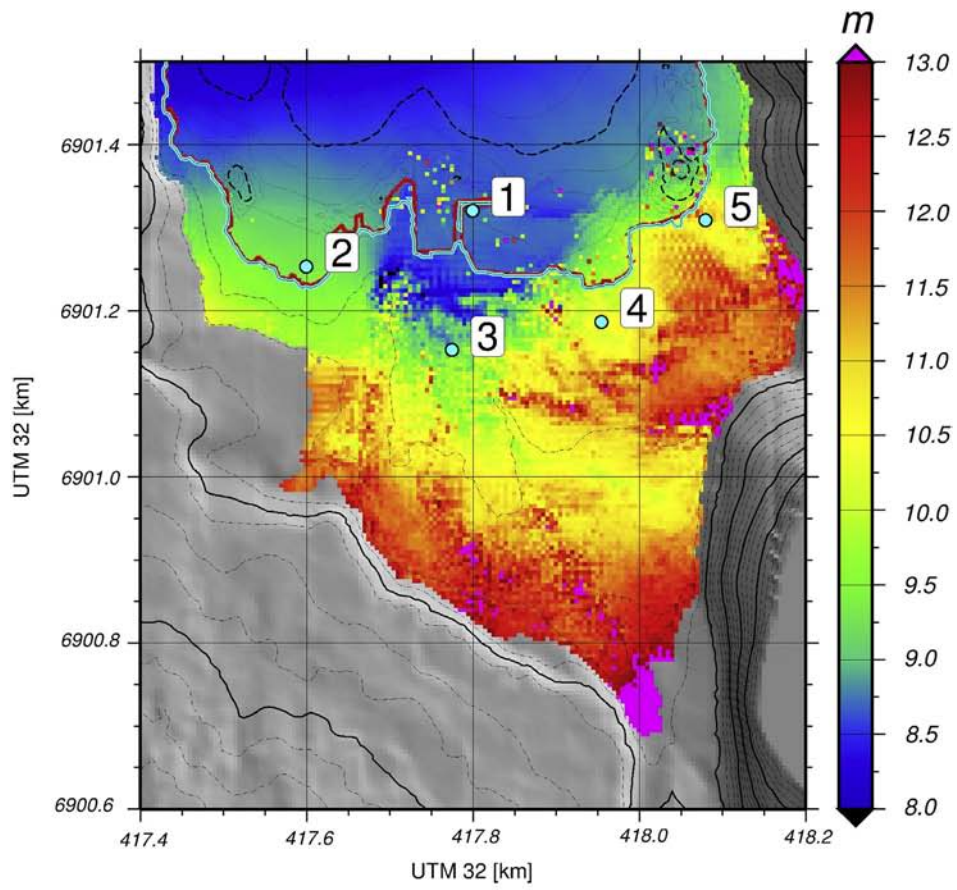


Fig. 18. Maximum inundation height (together with maximum surface elevation in the fjord) measured from 0.7 m above current mean sea level at Hellesylt, scenario 1C (nominal probability between 1 in 1000 and 1 in 5000 years). The red line is the shoreline for current mean sea level (MSL) while the cyan line is the shoreline including the estimated sea level rise of 0.7 m (the two shorelines are deduced from two different datasets (see Section 4.1), hence the latter somewhere erroneously ends up outside the first one). Contour lines are printed every 200 m. (For interpretation of the references to colour in this figure legend, the reader is referred to the web version of this article.)



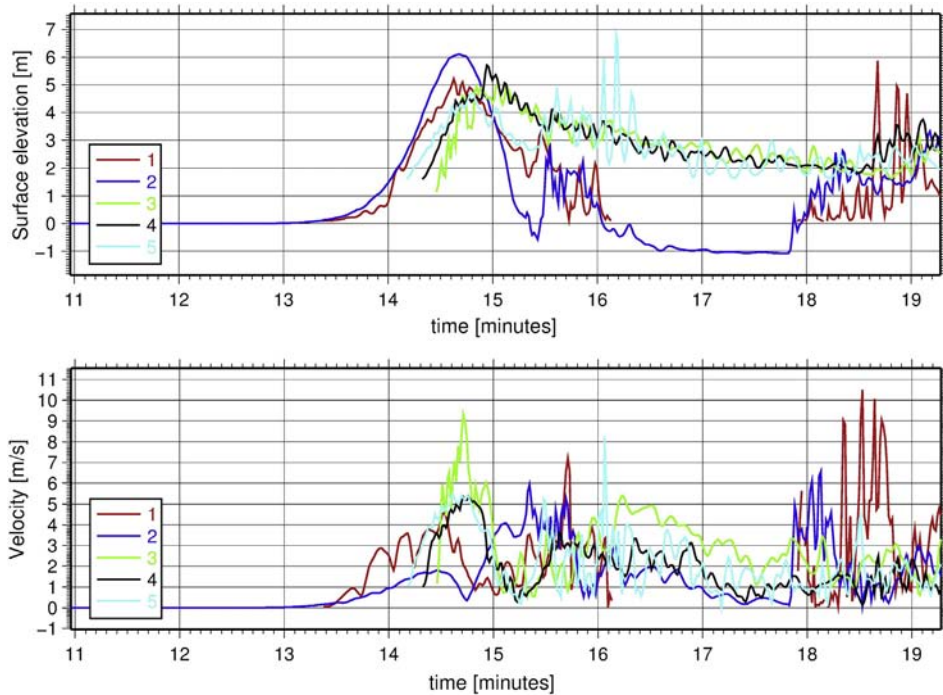


Fig. 20. Time history of the offshore surface elevation or onshore inundation height (m; upper panel) and current velocity (absolute values m/s; lower panel) measured from 0.7 m above current mean sea level at gauges 1–5 (see Fig. 19) at Tafjord for scenario 1C (nominal probability between 1 in 1000 and 1 in 5000 years).

momentum flux. The momentum flux may be interpreted as the drag force per unit width for a building or another surface-piercing stationary object vertically oriented over the flow depth (Yeh, 2006) and is normally suggested as the best damage indicator (Tsunami Pilot Study Working Group, 2006), but is more complicated to calculate and interpret. For simplicity, the present hazard study is mainly based on the maximum inundation height (the highest level reached by the water at each point of the inundation area measured above equilibrium water level during the tsunami impact). For completeness, also the maximum current velocity (the highest absolute value of the current velocity) and the maximum flow depth are computed to be used in possible later wave load calculations and design of constructions. Some locations were analysed in even more detail using time series of surface elevation and absolute current velocity.

The 23 locations considered here were defined by ÅTB (2009) to have the greatest need for hazard zonation, Fig. 3 and Table 1. The scenarios 1C and 2B in the Åkerneset rock slope are evaluated for all these locations. The scenarios H2 and H3 in the Hegguraksla rock slope are evaluated only for Fjåra, Vika, Tafjord, and Valldal. To give some examples, Fig. 3 first depicts the maximum surface elevation for scenario 1C calculated by the linear dispersive propagation model. Secondly, the trimlines (lines of maximum inundation distance) at Hellesylt for the two rockslide scenarios at Åkerneset (1C, 2B) and the trimlines at Tafjord for rockslide scenarios both at Åkerneset and Hegguraksla (1C, 2B, H2, H3) are given in Figs. 16 and 17, respectively. Further, maximum inundation heights for scenario 1C are depicted in Fig. 18 (Hellesylt) and Fig. 19 (Tafjord) together with maximum surface elevation in the fjord. The latter figure also shows maximum current velocities at Tafjord. Time histories for the inundation heights (and surface elevation) and the current velocity are exemplified for scenario 1C at Tafjord in Fig. 20. The flow depth at Tafjord is shown in Fig. 21. Finally, longitudinal transects of the incident wave at Hellesylt, Geiranger, and Tafjord are illustrated for scenario 1C in Fig. 22. It should be noted that the front of

the incident wave is fairly gentle. An almost vertical bore front that allows for breaking is not formed until the wave reaches the shoreline or even later. Similar features were observed in the simulations by R.E. Bredesen (NGI, 2010a, Appendix B).

The maximum calculated run-up heights for all 23 locations are summarized in Table 1. Highest run-up is expected for waves impacting the shore perpendicularly. This typically happens in the heads of the fjord system, which are at the same time normally the most inhabited locations. Here the tsunami may also be amplified due to gentle slope shoaling and possible focusing (as may be seen from simple considerations of energy flux; see Mei (1989) for details on Green's law). Reduction of run-up height with increasing angle of incidence is discussed by Pedersen (2011). The reduction of run-up heights for solitons is not much pronounced as long as the angle of incidence is less than 45°. Possible wave breaking also reduces the potential run-up height through energy dissipation, but may locally lead to stronger damage.

The examples further demonstrate large local variations of both maximum inundation height and maximum current velocity. The maximum current velocity may be obtained during withdrawal, and on either side (onshore or offshore) of the original shoreline. The Tsunami Pilot Study Working Group (2006) confirms that the flow depth remains small, but the current speed can be substantial during run-down. Topographic channelling may also cause higher current velocities. This is seen in the simulations for Stordal, Stranda, and Valldal (NGI, 2010a) and weakly for Tafjord, Fig. 21. Attempts should be made to avoid such channelling when designing obstructions against a potential tsunami.

6. Tsunami hazard and risk analysis

The unstable rock slopes at Åkerneset and Hegguraksla are situated in remote steep-mountain areas along deep fjords, and the risk is related to destructive rockslide tsunamis. The inundation simulations provide a more accurate description of the impacted area and the flow

Fig. 19. Maximum inundation height (together with maximum surface elevation in the fjord) measured from 0.7 m above current mean sea level (upper panel) and maximum velocity (lower panel) at Tafjord, scenario 1C (nominal probability between 1 in 1000 and 1 in 5000 years). The red line is the shoreline for current mean sea level (MSL) while the cyan line is the shoreline including the estimated sea level rise of 0.7 m. Contour lines are printed every 200 m. (For interpretation of the references to colour in this figure legend, the reader is referred to the web version of this article.)

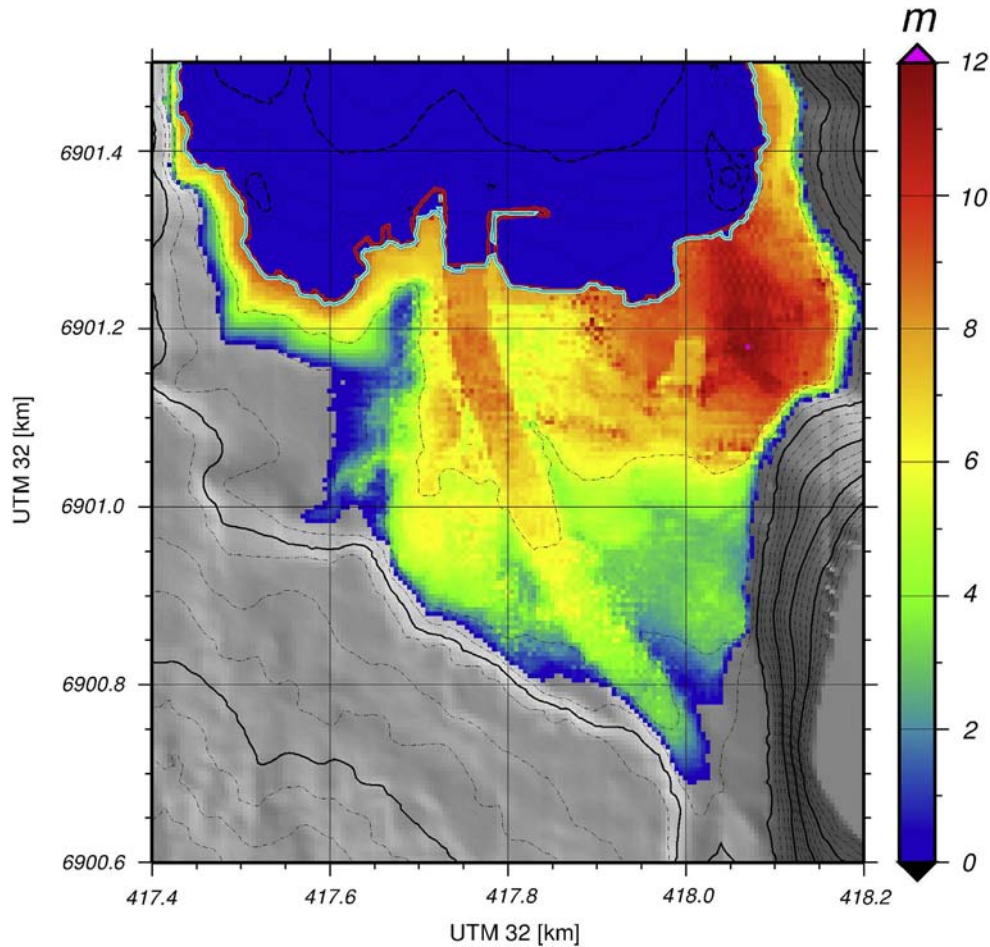


Fig. 21. Maximum flow depth at Tafjord for scenario 1C (nominal probability between 1 in 1000 and 1 in 5000 years) given in metres. The heights include the effect of a sea level rise of 0.7 m. The red line is the shoreline for current mean sea level (MSL) while the cyan line is the shoreline including the estimated sea level rise of 0.7 m. (For interpretation of the references to colour in this figure legend, the reader is referred to the web version of this article.)

field of each scenario (with a corresponding probability, i.e. the hazard). Combined with existing tools for local tsunami vulnerability and risk analysis, this enables a more detailed mapping of the elements at risk (population, buildings, infrastructure, etc.). Several works describe such rockslide tsunami risk analysis approaches for Storfjorden. Eidsvig et al. (2009) present a simple, practical, and quantitative method for estimating the risk due to a potential tsunamigenic rockslide and for illustrating uncertainty propagation through the steps in the risk analysis. Eidsvig and Medina-Cetina (2008) apply a Bayesian Network (Medina-Cetina and Nadim, 2008) that incorporates causal effects and has the capacity to back-propagate evidence to find a diagnosis (diagnosis analysis results for prescribed risk levels could be a useful tool during operation of an early-warning system). Lacasse et al. (2008) analyse the risk by event tree analysis (especially useful for geotechnical problems that involve large uncertainties).

The final risk assessment was made on a political level. It was found that the rockslide tsunami hazard (probability of impact) is higher than accepted by the Norwegian Planning and Building Act, which should at that time prevent any further development in all the exposed areas of the entire fjord system. This would obviously represent a serious drawback for a region that to a large extent lives from coastal and maritime activities. Advantages and disadvantages of a more dynamic approach to the problem are discussed by Agenda (2008). The Act is today altered to open for specified further development in the various hazard zones. However, this is only accepted if there are no alternative appropriate areas, physical safety measures are assessed, critical facilities are not located in the most hazardous zones, a reliable early-warning system

providing a minimum of 72 hours warning is implemented, and evacuation plans as well as public awareness and preparedness are elaborated.

As a result, the tsunami hazard analyses described above were applied for risk management in terms of hazard map production and land-use planning. The larger and less probable scenarios 1C and H3 were applied for evacuation zones and routes, Fig. 23. The smaller and more probable scenarios 2B and H2 were applied for location and design of less critical facilities accepted in the corresponding inundation zone. Also an operational tsunami early-warning system was designed. This system is managed by the Åknes/Tafjord Beredskap IKS preparedness centre and based on the fact that large rockslides normally give pre-failure signals. When motions in the rock slope pass certain threshold values, warnings are disseminated by air horns and cell phones (Blikra, 2012). The awareness of the people is ensured by evacuation drills (<http://www.fylkesmannen.no/hoved.aspx?m=1566&amid=2319864>) as well as comprehensive information and education of key personnel. Preparations for and actions to be performed under acute situations are detailed (in Norwegian) at the internet pages www.aknes.no of the preparedness centre.

7. Concluding remarks and further studies

Tsunami hazard and risk in a complex fjord system are analysed through a multidisciplinary approach spanning from rockslide source analysis to tsunami risk management in Storfjorden, western Norway. A comprehensive rock-slope-monitoring system is described. The

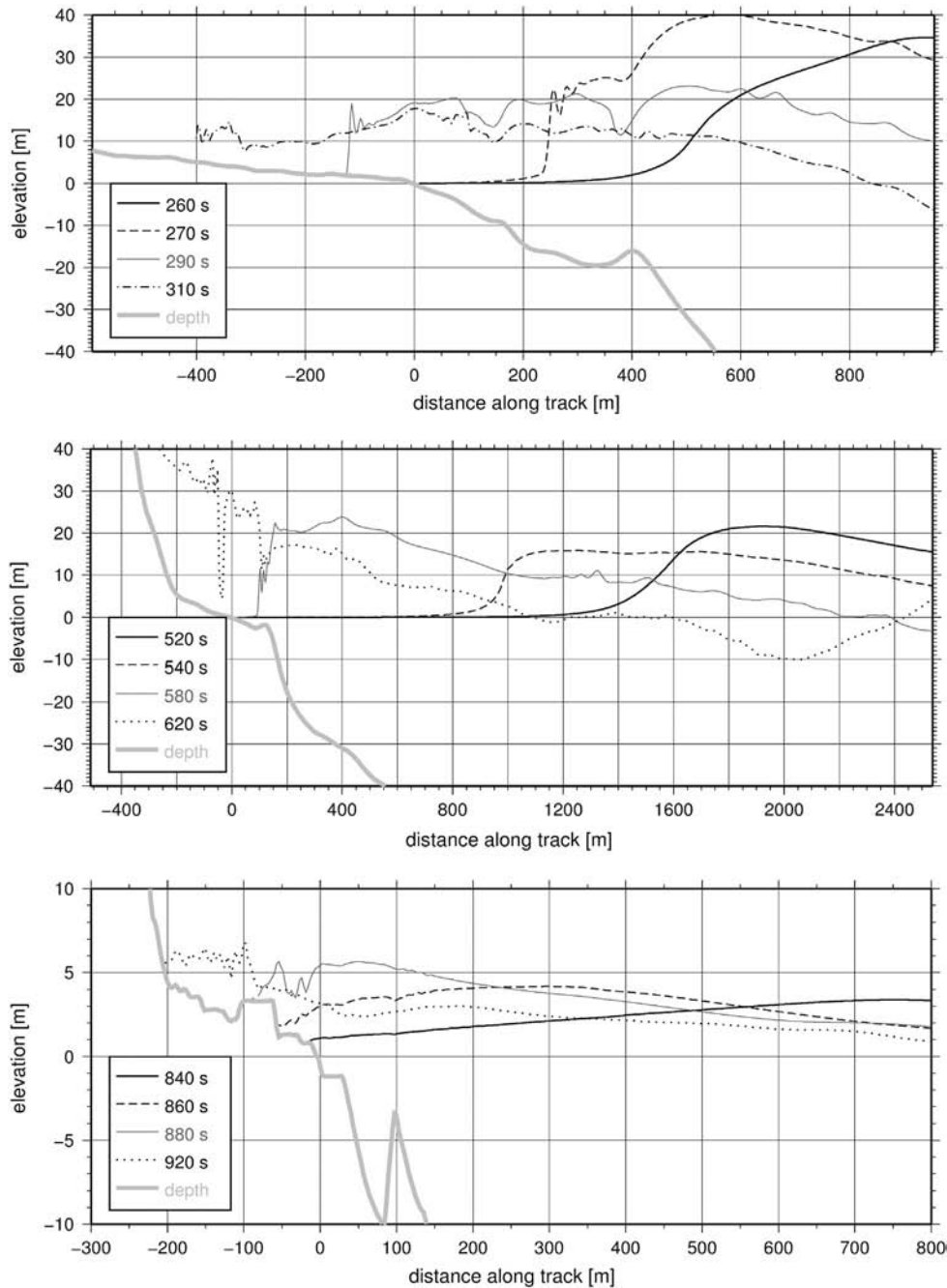


Fig. 22. Longitudinal transects of the incident wave at Hellesylt (upper panel), Geiranger (mid panel), and Tafjord (lower panel) for scenario 1C (nominal probability between 1 in 1000 and 1 in 5000 years). The location of the transects is shown in Fig. 7. 20× vertical exaggeration.

geoscientific investigations have established four rockslide scenarios (with corresponding annual probabilities of release) applied as input to the tsunami simulations. Inundation modelling and hazard zoning are performed for more than twenty locations and applied for land-use planning.

Two computational models are applied for the generation/propagation phase and a third model for the inundation phase. The models are validated by parameter sensitivity analyses, observations from two- and three-dimensional laboratory experiments, comparisons with other computational models, and back-calculations of historical events. The best match between the numerical simulations and the laboratory experiments is found for the larger scenarios (involving less pronounced scale effects) with the linear dispersive solution for the propagation phase; the corresponding calculated run-up values are

remarkably similar to the ones observed during the laboratory experiments.

Highest run-up is obtained where the waves impact the shore perpendicularly. This occurs in particular in the heads of the fjord system, where amplification due to gentle slope shoaling and possible focusing is also favoured. These areas are at the same time the most inhabited ones. The results further demonstrate large local variations of both maximum inundation height and maximum current velocity. The uncertainties are mainly related to how the rockslides will enter the water in a real event. In the numerical calculations, a “credible worst case configuration” is applied for each volume.

The present findings of the Åknes/Tafjord project and the existing and unique 1:500-scale fjord model established by SINTEF Coast and Harbour Research Laboratory (CHL) form an excellent starting point



Fig. 23. Example of hazard map for tsunamis from a potential rockslide at Åkerneset impacting Stranda, Sunnlyvsfjorden. Hazard zone up to 10 m.a.s.l. (produced by the Åknes/Tafjord project).

for additional and required basic research on rockslide tsunamis in fjords. Extended work to establish procedures and facilitate operational models for analysis of possible future rockslide tsunamis is presently performed by the Department of Mathematics at the University of Oslo (UiO), the Norwegian Geotechnical Institute (NGI), and CHL. Coupling of various mathematical models for rockslide generation, propagation, and run-up of waves is emphasized. The cooperation is granted by the FRITEK programme of the Research Council of Norway (RCN) for 2011–2014.

Finally, a system for rapid tsunami early warning by seabed pressure sensors should be elaborated. Seabed pressure sensors may serve as an alternative (or addition) to vulnerable monitoring systems in unstable rock slopes. Such sensors will be able to detect all possible tsunamis in a fjord or a lake (not only those emerging from a release in already-monitored rock slopes), they can be applied to confirm or cancel warnings issued by other (less reliable) systems, and they will provide valuable records in case of a real full-scale event. Even though the warning time in fjords and lakes is short (from a few to some tens of minutes), such a system will be significantly better than no warning at all.

Acknowledgements

The present paper is mostly based on R&D work and consulting funded by the Åknes/Tafjord project and Åknes/Tafjord Beredskap IKS from 2005 to 2011. The RCN FRITEK project “Laboratory experiments and numerical modelling of tsunamis generated by rockslides into fjords” (contract no. 205184/V30), the Department of Mathematics at the University of Oslo, the Norwegian Geotechnical Institute, and the International Centre for Geohazards (ICG) are all thanked for supporting the conversion of the NGI reports for the Åknes/Tafjord project into this journal paper. L.H. Blikra is thanked for the valuable advices throughout the consulting project, for the comments on the present paper, and for producing Fig. 4. G. Kaiser is thanked for producing the

lower panel of Fig. 14. U.M.K. Eidsvåg is thanked for the information on risk analysis for the Åkerneset rockslide and tsunami. D. Long and M. Vanneste are thanked for the helpful discussions on the NE Atlantic tsunami hazard. Finally, R. Weiss and another anonymous reviewer are thanked for the highly valuable comments to the manuscript. This is contribution no. 431 of the International Centre for Geohazards.

References

- Abadie, S., Morichon, D., Grilli, S., Glockner, S., 2010. Numerical simulation of waves generated by landslides using a multiple-fluid Navier–Stokes model. *Eng. Geol.* 57, 779–794.
- Agenda, 2008. Utbygging i fareområder — samfunnsøkonomiske vurderinger av reguleringsregimet langs Storfjorden på Sunnmøre. Report no. R6285 (in Norwegian). <http://www.regjeringen.no/upload/KRD/Vedlegg/BOBY/rapporter/utbyggingfareomr.pdf>.
- Alfnes, E., Førland, E.J., 2006. Trends in extreme precipitation and return values in Norway 1900–2004. *met.no Report 2*, Oslo.
- Ataie-Ashtiani, B., Malek-Mohammadi, S., 2006. Near field amplitude of subaerial landslide generated waves in dam reservoirs. *Dam Engineering* XVII, 4, pp. 197–222.
- Ball, J.W., 1970. Hydraulic Model Studies, Wave Action Generated by Slides into Mica Reservoir. Report. Western Canada Hydraulic Laboratories Ltd., Vancouver.
- Bellotti, G., Di Risio, M., De Girolamo, P., 2009. Feasibility of tsunami early warning systems for small volcanic islands. *Nat. Hazards Earth Syst. Sci.* 9, 1911–1919.
- Benestad, R.E., 2013. Association between trends in daily rainfall percentiles and the global mean temperature. *J. Geophys. Res.* 118, 10802–10810.
- Blikra, L.H., 2012. The Åknes rockslide, Norway. In: Clague, J.J., Stead, D. (Eds.), *Landslides: Types, Mechanisms and Modeling*. Cambridge University Press, pp. 323–335.
- Blikra, L.H., Longva, O., Harbitz, C.B., Løvholt, F., 2005. Quantification of rock-avalanche and tsunami hazard in Storfjorden, western Norway. In: Senneset, K., Flaate, K., Larsen, J.O. (Eds.), *Landslides and Avalanches*. Proceedings of the 11th International Conference and Field Trip on Landslides, Norway, 1–10 September 2005. Taylor & Francis Group, London, pp. 57–63.
- Blikra, L.H., Longva, O., Braathen, A., Anda, E., Dehls, J., Stalsberg, K., 2006. Rock-slope failures in Norwegian fjord areas: examples, spatial distribution and temporal pattern. In: Evans, S.G., Scarawcia Mugnozza, G., Strom, A.L., Hermanns, R.L. (Eds.), *Landslides from Massive Rock Slope Failure*. Nato Science Series IV, Earth and Environmental Sciences, 49, pp. 475–496.
- Braathen, A., Blikra, L.H., Berg, S.S., Karlsen, F., 2004. Rock-slope failures in Norway: type, geometry, deformation mechanisms and stability. *Norw. J. Geol.* 84, 67–88.

- Bungum, H., Lindholm, C., 2007. Tsunamigenic seismic sources in the North Sea, the Norwegian continental margin and the Norwegian–Greenland Sea. NORSAR report October 2007.
- BWG, 2002a. Sicherheit der Stauanlagen. Richtlinien des BWG Version 1.1. <http://www.bfe.admin.ch/stauanlagen>.
- BWG, 2002b. Sicherheit der Stauanlagen. Basisdokumentation zu Überwachung und Unterhalt Version 1.0. <http://www.bfe.admin.ch/stauanlagen>.
- Chaudhry, M.H., Mercer, A.G., Cass, D., 1983. Modeling of slide-generated waves in a reservoir. *J. Hydraul. Eng.* 109 (11), 1505–1520.
- ComMIT, 2011. Community Model Interface for Tsunami. <http://nctr.pmel.noaa.gov/ComMIT/>.
- Davidson, D.D., McCartney, B.L., 1975. Water waves generated by landslides in reservoirs. *J. Hydraul. Div. Proc. ASCE* 101 (HY12), 1489–1501.
- Davidson, D.D., Whalin, R.W., 1974. Potential landslide-generated water waves, Libby Dam and Lake Koocanusa, Montana. Technical Report H-74-15, Waterway Experiment Station, U.S. Army Corps of Engineers, Vicksburg, Miss.
- Derron, M.-H., Blikra, L.H., Jaboyedoff, M., 2005. High resolution digital elevation model analyses for landslide hazard assessment (Åkerneset, Norway). In: Senneset, K., Flaate, K., Larsen, J.O. (Eds.), *Landslides and Avalanches. Proceedings of the 11th International Conference and Field Trip on Landslides, Norway, 1–10 September 2005*. Taylor & Francis Group, London.
- Droz, P., Spasic-Gril, L., 2006. Lake Sarez risk mitigation project: a global risk analysis. International Congress on Large Dams, Barcelona, 2006 (http://www.stucky.ch/en/contenu/pdf/c_5_1.pdf).
- DSB, 2009. Havnivåstigning: Estimer av framtidig havnivåstigning i norske kystkommuner. Revidert utgave. Utgitt av: Det nasjonale klimatilpassingssekretariat ved Direktoratet for samfunnssikkerhet og beredskap (in Norwegian).
- Dyrørdal, A.V., Isaksen, K., Hygen, H.O., 2011. Past changes in frequency, intensity, and spatial occurrence of meteorological triggering variables relevant for natural hazards in Norway. *met.no Report 3*, Oslo.
- Dyrørdal, A.V., Isaksen, K., Hygen, H.O., Meyer, N.K., 2012. Changes in meteorological variables that can trigger natural hazards in Norway. *Clim. Res.* 55, 153–165.
- Eidsvåg, U., Medina-Cetina, Z., 2008. Quantitative risk assessment for tsunamigenic rock slides: the Åknes case study. ICG Report 2006-2-3 for the EU Project IRASMOG. Norwegian Geotechnical Institute, Oslo.
- Eidsvåg, U., Medina-Cetina, Z., Kveldsvik, V., Glimsdal, S., Harbitz, C.B., Sandersen, F., 2009. Risk assessment of a tsunamigenic rockslide at Aaknes. *Nat. Hazards*. <http://dx.doi.org/10.1007/s11069-009-9460-6>.
- Eie, J., Solberg, G., Tvinnereim, K., Tørum, A., 1971. Waves generated by landslides. Proceedings From the First International Conference on Port and Ocean Engineering Under Arctic Conditions. NTH, Trondheim, pp. 489–513.
- Eneqren, E.G., Imrie, A.S., 1996. Ongoing requirements for monitoring and maintaining a large remediated rockslide. Proceedings of the 7th International Symposium on Landslides, Trondheim, Norway, 17–21 June 1996. Balkema, pp. 1677–1682.
- Engen-Skaugen, T., Førland, E.J., 2011. Future changes in extreme precipitation estimated in Norwegian catchments. *met.no Report 13*, Oslo.
- Fritz, H.M., 2002. Initial phase of landslide generated impulse waves. VAW Mitteilung 178Versuchsanstalt für Wasserbau, Hydrologie und Glaziologie, ETH Zürich.
- Fritz, H.M., Hager, W.H., Minor, H.-E., 2001. Lituya Bay case: rockslide impact and wave run-up. *Sci. Tsunami Hazards* 19 (1), 3–22.
- Fritz, H.M., Hager, W.H., Minor, H.-E., 2003a. Landslide generated impulse waves 1. Instantaneous flow fields. *Exp. Fluids* 35, 505–519.
- Fritz, H.M., Hager, W.H., Minor, H.-E., 2003b. Landslide generated impulse waves 2. Hydrodynamic impact craters. *Exp. Fluids* 35, 520–532.
- Fritz, H.M., Hager, W.H., Minor, H.-E., 2004. Near field characteristics of landslide generated impulse waves. *J. Waterw. Port Coastal Ocean Eng.* 130 (6), 287–302.
- Fritz, H.M., Mohammed, F., Yoo, J., 2009. Lituya Bay landslide impact generated megatsunami 50th anniversary. *Pure Appl. Geophys.* 166, 153–175.
- Furseth, A., 1985. *Dommedagsfjellet – Tafjord 1934*. Gyldendal Norsk Forlag, Oslo (in Norwegian)82-05-16413-4.
- Furseth, A., 2006. *Skredulykker i Norge*. Tun Forlag (in Norwegian)82-529-3043-3.
- Furseth, A., 2009. *Dommedagsfjellet – Tafjordulykka 75 år etter*. Det Norske Samlaget (in Norwegian)978-82-521-7376-5.
- Furseth, A., 2012. *Farlige bølger. Vigmostad & Bjørke* (in Norwegian)978-82-419-0851-4.
- Galster, R.W., 1991. Landslides near abutments of three dams in the Pacific Northwest, USA. In: Bell (Ed.), *Landslides*. Balkema, Rotterdam, pp. 1241–1248.
- Ganerød, G.V., Grøneng, G., Rønning, J.S., Dalsegg, E., Elvebakk, H., Tønnesen, J.F., Kveldsvik, V., Eiken, T., Blikra, L.H., Braathen, A., 2008. Geological model of the Åknes rockslide, western Norway. *Eng. Geol.* 102, 1–18.
- George, D.L., LeVeque, R.J., 2006. Finite volume methods and adaptive refinement for global tsunami propagation and local inundation. *Sci. Tsunami Hazards* 24, 319–328.
- Ghirotti, M., 2012. The 1963 Vaiont landslide, Italy. In: Clague, J.J., Stead, D. (Eds.), *Landslides: Types, Mechanisms and Modeling*. Cambridge University Press, pp. 359–372.
- Hanssen-Bauer, I., Drange, H., Førland, E.J., Roald, L.A., Børsheim, K.Y., Hisdal, H., Lawrence, D., Nesje, A., Sandven, S., Sorteberg, A., Sundby, S., Vasskog, K., Ådlandsvik, B., 2009. *Klima i Norge 2100 – Bakgrunnsmateriale til NOU Klimatilpassing*. Oslo (in Norwegian).
- Harbitz, C., 1988. Numerisk Modellering av Skredgenererte Flodbølger. Master Thesis University of Oslo (in Norwegian).
- Harbitz, C.B., 1992. Reflection–transmission of nonlinear waves in channel bends. *Applied Mathematics No. 6*, April 1992Preprint series, Inst. of Mathematics, University of Oslo82-553-0775-3.
- Harbitz, C., Pedersen, G., Gjevik, B., 1993. Numerical simulations of large water waves due to landslides. *J. Hydraul. Eng.* 119, 1325–1342.
- Harbitz, C.B., Domaas, U., Varlid, E., 2001. Flodbølger etter fjellskred – Sannsynlighet og faresoner i Åfjorden, Hyllestad. Norsk Jord og Fjellteknisk Forbund, Bergmekanikkdagen 23. November 2001, Oslo (in Norwegian with English abstract).
- Harbitz, C.B., Glimsdal, S., Løvholt, F., Pedersen, G.K., Vanneste, M., Eidsvåg, U.M.K., Bungum, H., 2009. Tsunami hazard assessment and early warning systems for the North East Atlantic. Proceedings of the DEWS Midterm Conference 2009, Potsdam, Germany, 7–8 July 2009.
- Harbitz, C.B., Glimsdal, S., Bazin, S., Zamora, N., Smebye, H.C., Løvholt, F., Bungum, H., Gauer, P., Kjekstad, O., 2012. Tsunami hazard in the Caribbean: regional exposure derived from credible worst case scenarios. *Cont. Shelf Res.* 38, 1–23 (<http://www.sciencedirect.com/science/article/pii/S0278434312000349>).
- Hermanns, R.L., Oppikofer, T., Anda, E., Blikra, L.H., Böhme, M., Bunkholt, H., Crosta, G.B., Dahle, H., Devoli, G., Fischer, L., Jaboyedoff, M., Loew, S., Sætre, S., Yugi Molina, F.X., 2013a. Hazard and risk classification for large unstable rock slopes in Norway. Proceedings of the International Conference Vajont 1963–2013, Padua, Italy, 8–10 October 2013. Italian Journal of Engineering Geology and Environment – Book Series 6 (www.ijege.uniroma1.it).
- Hermanns, R.L., Oppikofer, T., Dahle, H., Eiken, T., Ivy-Ochs, S., Blikra, L.H., 2013b. Understanding long-term slope deformation for stability assessment of rock slopes: the case of the Oppstadhornet rockslide, Norway. Proceedings of the International Conference Vajont 1963–2013, Padua, Italy, 8–10 October 2013. Italian Journal of Engineering Geology and Environment – Book Series 6 (www.ijege.uniroma1.it).
- Hov, Ø., Cubasch, U., Fischer, E., Höppe, P., Iversen, T., Kvamstø, N.G., Kundzewicz, Z.W., Rezacova, D., Rios, D., Santos, F.D., Schädel, B., Veisz, O., Zerefos, C., Benestad, R., Murlis, J., Donat, M., Leckebusch, G.C., Ulbrich, U., 2013. Extreme Weather Events in Europe: Preparing for Climate Change Adaptation. Norwegian Meteorological Institute, Oslo978-82-7144-100-5 (136 pp.).
- Huber, A., 1982. Impulse waves in Swiss lakes as a result of rock avalanches and bank slides. Experimental Results for the Prediction of the Characteristic Numbers of These Waves. Proceedings of the 14th Congress on Large Dams Q54, R29, pp. 455–476.
- Huber, A., Hager, W.H., 1997. Forecasting impulse waves in reservoirs. Proceedings of the 19th Congress On Large Dams C31, Florence, Italy, pp. 993–1005.
- ICOLD, 2002. Reservoir Landslides: Investigation and Management – Guidelines and Case Histories. International Commission on Large Dams Bulletin, p. 124.
- Imrie, A.S., Moore, D.P., Eneqren, E.G., 1991. Performance and maintenance of the drainage system at Downie Slide. Proceedings of the 6th International Symposium on Landslides, Christchurch, New Zealand, 10–14 February 1992. Balkema, pp. 751–757.
- Jensen, A., Sælevik, G., Pedersen, G., 2007. 2D Experimental Investigation of the Wave Impact From the Potential Åknes Rock Slide. University of Oslo, Department of Mathematics (report October 2007).
- Jørstad, F., 1968. Waves Generated by Landslides in Norwegian Fjords and Lakes. Norwegian Geotechnical Institute publ. p. 79.
- Kalenchuk, K.S., Hutchinson, D.J., Diederichs, M., Moore, D., 2012. Downie slide, British Columbia, Canada. In: Clague, J.J., Stead, D. (Eds.), *Landslides: Types, Mechanisms and Modeling*. Cambridge University Press, pp. 345–357.
- Kamphuis, J.W., Bowering, R.J., 1970. Impulse waves generated by landslides. Proceedings of the 12th Coastal Engineering Conference ASCE 1, pp. 575–588.
- Kiersch, G.A., 1964. Vaiont reservoir disaster. *Civ. Eng.* 34, 32–39.
- Kveldsvik, V., Einstein, H.H., Nilsen, B., Blikra, L.H., 2009. Numerical analysis of the Åknes rock slope based on measured displacements and geotechnical data. *Rock Mech. Rock Eng.* 42, 689–728.
- Lacasse, S., Eidsvåg, U., Nadim, F., Høeg, K., Blikra, L.H., 2008. Event tree analysis of Åknes rock slide hazard. 4th Canadian Conference on Geohazards, Quebec Canada, May 2008.
- Langtangen, H.P., Pedersen, G., 1998. Computational models for weakly dispersive and nonlinear water waves. *Comput. Methods Appl. Mech. Eng.* 160, 337–358.
- Lauknes, T.R., Piyush Shanker, A., Dehls, J.F., Zebker, H.A., Henderson, I.H.C., Larsen, Y., 2010. Detailed rockslide mapping in northern Norway with small baseline and persistent scatterer interferometric SAR time series methods. *Remote Sens. Environ.* 114, 2097–2109.
- Lawrence, M.S., Roberts, N.J., Clague, J.J., 2013. The 2007 Chehalis Lake landslide, British Columbia: a landslide-generated surge wave (tsunami) with implications for dam safety. Proceedings of the GeoMontreal 2013 Conference, Montreal, Canada, 29 September–3 October 2013.
- Løvholt, F., Pedersen, G., 2009. Instabilities of Boussinesq models in non-uniform depth. *Int. J. Numer. Methods Fluids* 61 (6), 606–637.
- Løvholt, F., Pedersen, G., Gisler, G., 2008. Oceanic propagation of a potential tsunami from the La Palma Island. *J. Geophys. Res.* 113, C09026.
- Løvholt, F., Pedersen, G., Glimsdal, S., 2010. Coupling of dispersive tsunami propagation and shallow water coastal response. In: Zahibo, N., Pelinovsky, E., Yalciner, A., Titov, V. (Eds.), Proceedings of the “Caribbean Waves 2008” Workshop in Guadeloupe, December 2008. The Open Oceanography Journal, 4, pp. 71–82.
- Løvholt, F., Lynett, P., Pedersen, G., 2013. Simulating run-up on steep slopes with operational Boussinesq models; capabilities, spurious effects and instabilities. *Nonlinear Process. Geophys.* 20, 379–395.
- Lynett, P.J., Borrero, J.C., Liu, P.L.-F., Synolakis, C.E., 2003. Field survey and numerical simulations: a review of the 1998 Papua New Guinea tsunami. *Pure Appl. Geophys.* 160, 2119–2146.
- Macfarlane, D.F., 2009. Observations and predictions of the behaviour of large, slow-moving landslides in schist, Clyde Dam reservoir, New Zealand. *Eng. Geol.* 109, 5–15.
- Mader, C.L., 1999. Modelling the 1958 Lituya Bay mega-tsunami. *Sci. Tsunami Hazards* 17 (2), 57–67.
- Mader, C.L., 2004. Numerical Modelling of Water Waves, 2nd edition. CRC press LLC, Boca Raton, Florida (275 pp.).
- Medina-Cetina, Z., Nadim, F., 2008. Stochastic design of an early warning system. *Georisk* 2 (4), 223–236.

- Mei, C.C., 1989. The applied dynamics of ocean surface waves. Advanced Series on Ocean Engineering 1 World Scientific, London.
- Müller, D.J., 1960. Giant waves in Lituya Bay, Alaska. U.S. Geol. Surv. Prof. Pap. 354-C, 51–84.
- Müller, L., 1964. The rock slide in the Vaiont Valley. Rock Mech. Eng. Geol. 2, 148–212.
- Müller, L., 1968. New considerations on the Vaiont slide. Rock Mech. Eng. Geol. 6, 1–91.
- NGI, 1984. Statens Naturskadefond; Årdalstangen, Årdal kommune – Vurdering av fare for flodbølge ved skred i Kleppura. Norwegian Geotechnical Institute Report 83483-1 (in Norwegian).
- NGI, 1989. Kyrkjedøri, Terakamben; Aurland kommune, Sogn og Fjordane – Vurdering av faren for fjellskred. Norwegian Geotechnical Institute report 85465-1 (in Norwegian).
- NGI, 1991. Skredgenererte bølger fra Åkerneset – En modellanalyse av bølger mot Hellesylt. Norwegian Geotechnical Institute report 85494-4 (in Norwegian).
- NGI, 1992. Skredgenererte bølger – En teoretisk gjennomgang med praktiske eksempler. Norwegian Geotechnical Institute report 894031-1. (in Norwegian).
- NGI, 1999a. Hyllestad kommune – Vurdering av skredfare og bølgehøyder i Åfjorden. Norwegian Geotechnical Institute report 981014-1 (in Norwegian).
- NGI, 1999b. Osavatnet, Osterøy – Vurdering av skredfare og flodbølger. Norwegian Geotechnical Institute Report 994090-1 (in Norwegian).
- NGI, 2002. Ormen Lange – ilandføringsalternativer – Rock slide generated tsunamis – run-up heights at Baraldsnes and Nyhamn. Norwegian Geotechnical Institute report 20001472-2.
- NGI, 2003a. Tsunamis generated by rockslides in Geiranger- and Tafjorden – scenarios and model comparisons. Norwegian Geotechnical Institute Report 20011622-1.
- NGI, 2003b. Mysevatnet, Kvinnherad – Flodbølger etter fjellskred. Norwegian Geotechnical Institute Report 20031139-1 (in Norwegian).
- NGI, 2004a. Tsunami modellering and prediction – pre-project: slide-generated waves in reservoirs. Norwegian Geotechnical Institute Report 20031100-1.
- NGI, 2004b. Hotell og glassbjelke ved Zakariasdemningen – Vurdering av skredfare og skredgenererte bølger. Norwegian Geotechnical Institute Report 20031673-1 (in Norwegian).
- NGI, 2005. Nye Molde sykehus – Vurdering av oppskyllingshøyder. Norwegian Geotechnical Institute Report 20051159-1 (in Norwegian).
- NGI, 2006a. Fedafjorden, Kvinesdal kommune – Beregning av mulige fjellskred og flodbølger. Norwegian Geotechnical Institute Report 20061445-1 (in Norwegian).
- NGI, 2006b. The Åknes/Tafjord project – semi-annual report: preliminary results using an improved tsunami model. Norwegian Geotechnical Institute Report 20051018-1.
- NGI, 2008a. Flodbølge fra Åkneset – innvirkning på oppdrettsanlegg i Barstadvik, Møre – Beregning av oppskyllingshøyder. Norwegian Geotechnical Institute Report 20071923-1 (in Norwegian).
- NGI, 2008b. Flodbølge fra Åkneset – påvirkning på fiskeoppdrettsanlegg i Urke, Ørsta kommune. Norwegian Geotechnical Institute Report 20081633-1 (in Norwegian).
- NGI, 2008c. Flodbølge fra Åkneset – innvirkning på veier og fergekaier i Storfjorden, Møre – Generell orientering samt beregning av oppskyllingshøyder og bølgekrefter på Ørsneset fergekai. Norwegian Geotechnical Institute Report 20071856-1 (in Norwegian).
- NGI, 2008d. Flodbølger etter mulig fjellskred Nordnes, Lyngen kommune – Beregning av mulige fjellskred og flodbølger. Norwegian Geotechnical Institute Report 20071677-1 (in Norwegian).
- NGI, 2008e. The Åknes/Tafjord project – semi-annual report: tsunami impact in the outer part of Storfjorden, testing of numerical models for rock slide and tsunami, coupling to laboratory experiments. Norwegian Geotechnical Institute Report 20051018-2.
- NGI, 2009. Skred- og flodbølger ved Flåm, Aurland kommune – Beregning av flodbølger for tre potensielle fjellskred fra Stampa. Norwegian Geotechnical Institute Report 20081693-1 (in Norwegian).
- NGI, 2010a. The Åknes/Tafjord project – numerical simulations of tsunamis from potential and historical rock slides in Storfjorden; hazard zoning and comparison with 3D laboratory experiments. Norwegian Geotechnical Institute Report 20051018-00-1-R Rev. 01.
- NGI, 2010b. Sula kommune – flodbølger etter skred fra Åknes – Beregning av oppskylling ved Kvasnes, Vegsund og Solevågen. Norwegian Geotechnical Institute Report 20100247-00-3-R (in Norwegian).
- NGI, 2010c. Flodbølger etter mulig fjellskred Nordnes, Lyngen kommune II – Grovanalyse for et skredvolum på 22 millioner m³. Norwegian Geotechnical Institute Report 20100617-00-1-R (in Norwegian).
- NGI, 2011a. Hareid kommune – flodbølger etter skred fra Åknes – Beregning av oppskylling ved Brandal, Hareid sentrum og Hjørungavåg. Norwegian Geotechnical Institute Report 20100899-00-2-R (in Norwegian).
- NGI, 2011b. Ørsta kommune – flodbølger etter skred fra Åknes – Beregning av oppskylling. Norwegian Geotechnical Institute Report 20110232-00-1-R (in Norwegian).
- NGI, 2012. Ørskog kommune – flodbølgeberegninger Sjøholt – Beregning av oppskylling ved nytt bygg på gnr/bnr 97/162 og 97/404. Norwegian Geotechnical Institute Report 20120425-00-1-R (in Norwegian).
- NGI, 2013a. Impacts of extreme weather events on infrastructure in Norway (InfraRisk) – Sluttrapport til NFR-prosjekt 200689. Norwegian Geotechnical Institute Report 20091808-01-R (in Norwegian) (94 pp.).
- NGI, 2013b. Ørskog kommune – beregning av flodbølge ved Sjøholt. Sikringstiltak i Sjøholt sentrum. Norwegian Geotechnical Institute Report 20130150-01-R (in Norwegian).
- NGI, 2013c. Flodbølger i Lyngen etter mulig skred, Nordnes, Lyngen kommune III – Detaljberegning av oppskylling for skred på 11 millioner kubikkmeter. Norwegian Geotechnical Institute Report 20130206-01-R (in Norwegian).
- NGI, 2013d. Nye Molde sjukehus – nye vurderinger av flodbølger ved Hjelset. Detaljberegning av oppskylling etter mulig fjellskred fra Oppstadhornet. Norwegian Geotechnical Institute Report 20130612-01-R (in Norwegian).
- NGI, 2014. Evaluation of the flow characteristics of the potential Åkerneset rockslide, western Norway – contributions to the design of laboratory experiments on wave generation. Norwegian Geotechnical Institute Report 20061333-01-R.
- NGU, 2009a. Rock avalanches – distribution and frequencies in the inner part of Storfjorden, Møre og Romsdal County, Norway. Geological Survey of Norway Report 2009.002.
- NGU, 2009b. Faren for fjellskred fra Nordnesfjellet i Lyngenfjorden, Troms. Geological Survey of Norway Report 2009.026 (in Norwegian).
- NHL, 1983. Modellforsøk med rasgenererte bølger i Syngneskardsmagasinet. Norwegian Hydrodynamic Laboratories Report 603243 (in Norwegian).
- Noda, E., 1970. Water waves generated by landslides. J. Waterw. Harbours Coastal Eng. Div. ASCE 96 (WW4), 835–855.
- Nordvik, T., Blikra, L.H., Nyrnes, E., Derron, M.-H., 2010. Statistical analysis of seasonal displacements at the Nordnes rockslide, northern Norway. Eng. Geol. 114, 228–237.
- Oppikofer, T., 2010. Detection, Analysis and Monitoring of Slope Movements by High-resolution Digital Elevation Models. PhD thesis University of Lausanne.
- Pastor, M., Herreros, I., Fernández Merodo, J.A., Mira, P., Haddad, B., Quecedo, M., González, E., Alvarez-Cedrón, C., Drempetic, V., 2009. Modelling of fast catastrophic landslides and impulse waves induced by them in fjords, lakes, and reservoirs. Eng. Geol. 109, 124–134.
- Pedersen, G., 2011. Oblique runup of non-breaking solitary waves on an inclined plane. J. Fluid Mech. 668, 582–606.
- Pedersen, G., Løvholt, F., 2008. Documentation of a Global Boussinesq Solver. Mechanics and Applied Mathematics No. 1, February 2008. Department of Mathematics, University of Oslo, Norway (ISSN 0809-4403). <http://www.duo.uio.no/publ/matematikk/2008/124495/mech-01-08.pdf>.
- Perla, R.I., Cheng, T.T., McClung, D.M., 1980. A two-parameter model of snow-avalanche motion. J. Glaciol. 26 (94), 197–207.
- Piteau, D.R., Mylrea, F.H., Blown, I.G., 1978. Downie slide, Columbia River, British Columbia, Canada. In: Voight, B. (Ed.), Rockslides and Avalanches 1. Elsevier, New York, pp. 365–392.
- Raney, D.C., Butler, H.L., 1976. Landslide generated water wave model. J. Hydraul. Div. Proc. ASCE 102 (HY9), 1269–1282.
- Riemer, W., 1995. Keynote paper: landslides and reservoirs. In: Bell (Ed.), Landslides. Balkema, Rotterdam, pp. 1973–2004.
- Sælevik, G., Jensen, A., Pedersen, G., 2009. Experimental investigation of impact generated tsunami; related to a potential rock slide, Western Norway. Coastal Eng. 56, 897–906.
- Sánchez-Trejo, R., Espinosa, L., 1979. Rock slope movements with hydroelectric power projects, Mexico. In: Voight, B. (Ed.), Rockslides and Avalanches 2. Elsevier, New York, pp. 225–245.
- Schuster, R.L., Alford, D., 2004. Usoi landslide dam and Lake Sarez, Pamir Mountains, Tajikistan. Environ. Eng. Geosci. 2, 151–168.
- Semenza, E., 2005. La Storia del Vaiont, raccontata dal geologo che ha scoperto la frana, K-flash, 2nd ed. 978889288016 (Ferrara, Italy, 279 pp.).
- SINTEF, 2008. Notat – Rasmodell, Dated 2008-09-12 (in Norwegian).
- Slingerland, R.L., Voight, B., 1979. Occurrences, properties, and predict models of landslide-generated water waves. In: Voight, B. (Ed.), Rockslides and Avalanches 2. Elsevier, New York, pp. 317–397.
- Titov, V.V., 1997. Numerical Modeling of Long Wave Runup. PhD thesis University of Southern California.
- Titov, V.V., Synolakis, C.E., 1995. Modeling of breaking and nonbreaking long-wave evolution and runup using VTCS-2. J. Waterw. Port Coastal Ocean Eng. 121 (6), 308–316.
- Titov, V.V., Synolakis, C.E., 1998. Numerical modeling of tidal wave runup. J. Waterw. Port Coastal Ocean Eng. 124 (4), 157–171.
- Tsunami Pilot Study Working Group, 2006. Seaside, Oregon tsunami pilot study – modernization of FEMA flood hazard maps. NOAA OAR Special Report, NOAA/OAR/PMEL, Seattle, WA, 94 pp. +7 Appendices.
- Vanneste, M., Harbitz, C.B., De Blasio, F.V., Glimsdal, S., Mienert, J., Elverhøi, A., 2010. The Hinlopen-Yermak Landslide Arctic Ocean – geomorphology slide dynamics and tsunami simulations. In: Shipp, R.C., Weimer, P., Posamentier, H.W. (Eds.), The importance of mass-transport deposits in deepwater settings. SEPM Special Publication 95.
- VHL, 1967. Aurlandsutbyggingen – bølger ved ras i magasin. Delrapporter nr. 1–2. Vassdrags- og Havnelaboratoriet, SINTEF, Trondheim (in Norwegian).
- VHL, 1969. Rasgenererte bølger – Årdalsvatn. Delrapport nr. 1. Vassdrags og Havnelaboratoriet, SINTEF, Trondheim (in Norwegian).
- Voight, B., 1979. Wedge rockslides, Libby Dam and Lake Koocanusa, Montana. In: Voight, B. (Ed.), Rockslides and Avalanches 2. Elsevier, New York, pp. 281–315.
- Vorren, T.O., Mangerud, J., 2008. Glaciations come and go. In: Ramberg, I.B., Bryhni, I., Nøttvedt, A., Rangnes, K. (Eds.), The Making of a Land – Geology of Norway. Norsk Geologisk Forening, Trondheim, pp. 480–533.
- Vorren, T.O., Mangerud, J., Blikra, L.H., Nesje, A., Sveian, H., 2008. The emergence of modern Norway. In: Ramberg, I.B., Bryhni, I., Nøttvedt, A., Rangnes, K. (Eds.), The Making of a Land – Geology of Norway. Norsk Geologisk Forening, Trondheim, pp. 534–559.
- Weiss, R., Fritz, H.M., Wuennemann, K., 2009. Hybrid modeling of the mega-tsunami runup in Lituya Bay after half a century. Geophys. Res. Lett. 36, L09602.
- Wiegel, R.L., Noda, E.K., Kuba, E.M., Gee, D.M., Tornberg, G.F., 1970. Water waves generated by landslide in reservoirs. J. Waterw. Harbours Coastal Eng. Div. ASCE 96 (WW2), 307–333.
- Yeh, H., 2006. Tsunami forces in the runup zone. In: Mercado-Irizarry, A., Liu, P.L.-F. (Eds.), Caribbean Tsunami Hazard – Proceedings of the NSF Caribbean Tsunami Workshop. World Scientific Publishing Co. Pte. Ltd. ISBN: 981-256-535-3.
- Zweifel, A., Hager, W., Minor, H.-E., 2006. Plane impulse waves in reservoirs. J. Waterw. Port Coastal Ocean Eng. 132 (5), 358–368.
- ÅTB, 2009. Lokaltiteter og område for produksjon av detaljerte oppskyllingshøgder. Åknes/Tafjord Beredskap IKS v/Jarle Hole (in Norwegian).
- ÅTB, 2010a. Åknes: State of instrumentation and data analysis. Åknes report 02.2010. http://aknes.no/sites/default/files/Aaknesrapport02_2010.pdf.
- ÅTB, 2010b. Hegguraksla in Tafjorden: monitoring and data analysis. Åknes report 04.2010. http://aknes.no/sites/default/files/Aaknesrapport04_2010.pdf.
- ÅTB, 2011. Scenario og prognoser for fjellskred og flodbølger fra Åknes og Hegguraksla. Åknes Rapport 05.2011 (in Norwegian). http://aknes.no/sites/default/files/Aaknesrapport05_2011.pdf.